Published April 18, 2011

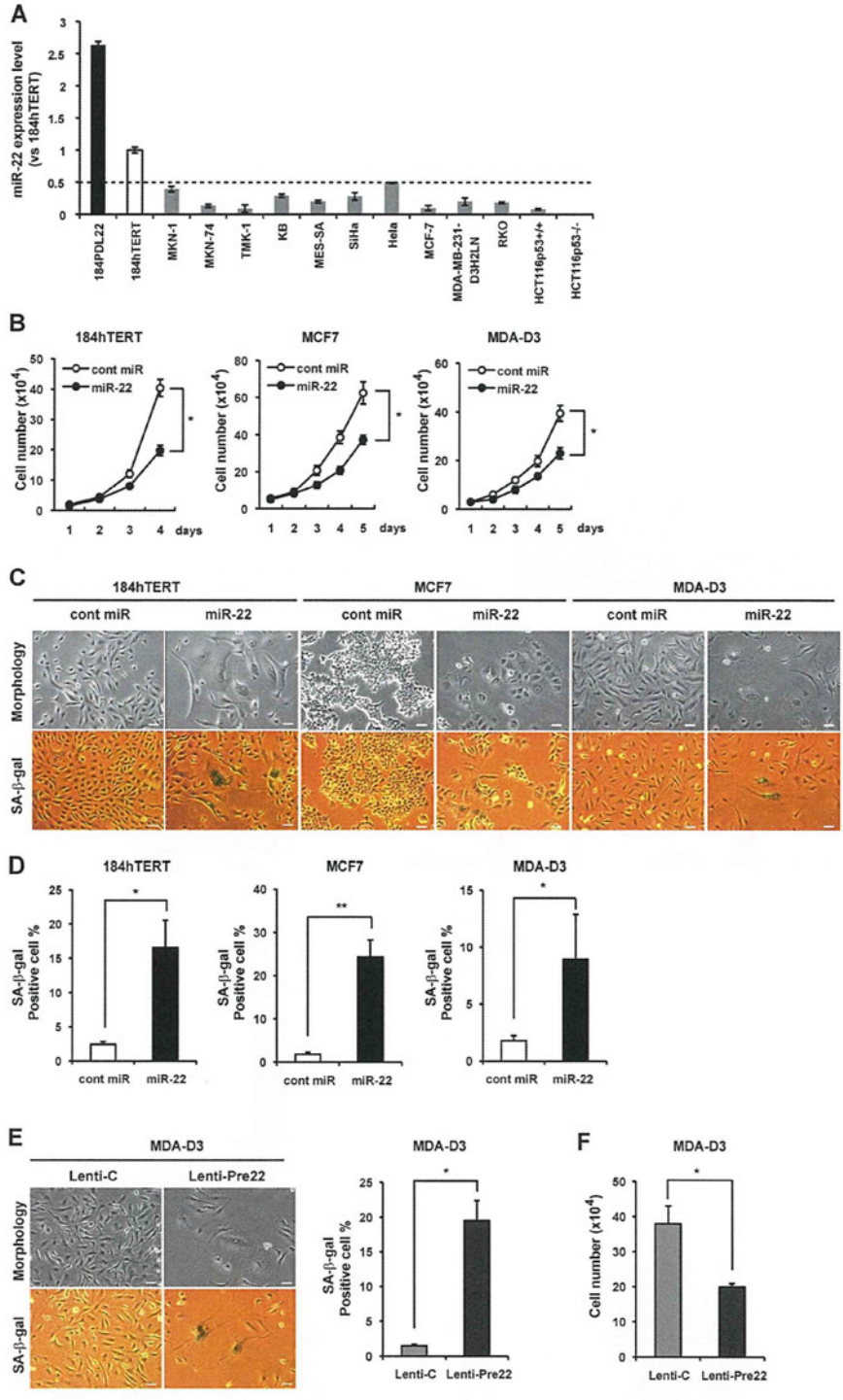

Figure 3. **Overexpression of miR-22 induces senescence-like phenotypes in human breast epithelial and breast cancer cells.** (A) qRT-PCR analysis shows relative quantitation of miR-22 expression level (vs. 184hTERT) in human epithelial and various cancer cells. Expression levels of miR-22 in various cells were relative to that in 184hTERT cells set at 1. U6 was used as an internal normalization control. The dashed line represents the threshold of expression level (0.5-fold vs. 184hTERT). (B) Cell proliferation assay was performed after transfection of miR-22, and cells were counted for the indicated days, compared with control cells. Each value was determined in triplicate. *, $P < 0.05$. (C–E) Cell morphology and SA-β-gal activity were analyzed by phase-contrast microscopy at day 6 after transfection (C and D) or infection (E) in indicated cells. SA-β-gal activity was presented by the percentage of SA-β-gal–positive cells. (F) Cell proliferation assay was performed at day 6 after MDA-D3 cells were infected with Lenti-Pre22 and compared with control cells. Data in all the panels represent mean ± SEM ($n = 3$). *, $P < 0.05$; **, $P < 0.01$. Bars, 50 µm.

(site 1 and site 3) reporters (Fig. 5 D), compared with the negative cont miR. In contrast, neither Mut1 (deletion of seed region) nor Mut2 of mutant reporters was repressed by miR-22, which indicates that these target sites directly mediate the repression (Fig. 5 E). In addition, this down-regulation was not seen in WT construct of CDK6 site 2, possibly because of poorly conserved sites among mammals. These results provide experimental evidence that miR-22 can directly repress translation initiation of SIRT1, SP1, and CDK6.

Western blot analysis showed that overexpression of miR-22 markedly down-regulated SIRT1, SP1, and CDK6 in SiHa and MDA-D3 cells (Fig. 5 F). Moreover, we confirmed that SIRT1 and CDK6 were down-regulated in senescent MRC-5 fibroblasts and HMEC184 epithelial cells, accompanied by a decrease in pRB phosphorylation at ser807/811 (Fig. 5 G). This indicates that SIRT1 and CDK6 are senescence-associated genes that are involved in cellular senescence possibly through the pRb pathway. Sp1 was not detected because of its low expression level in these cells.

Published April 18, 2011

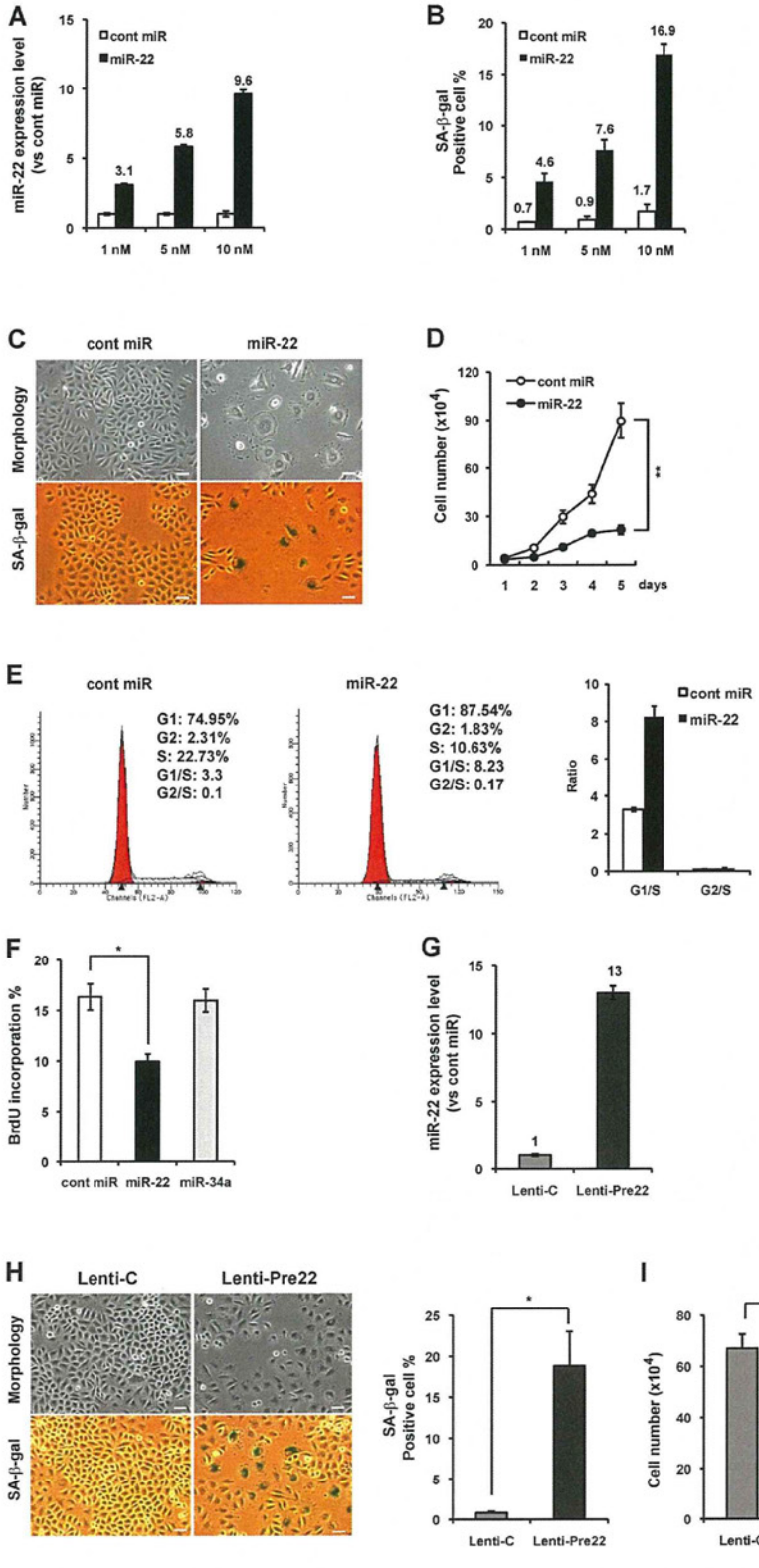

Figure 4. **Overexpression of miR-22 induced cellular senescence, cell cycle G1 arrest, and the decrease in BrdU incorporation in SiHa cells.** (A and B) SiHa cells were transfected with cont miR or miR-22 at the indicated concentration for 6 d. qRT-PCR results show the relative level of miR-22 expression to cont miR in each transfection group (A). SA-β-gal activity was presented by the percentage of SA-β-gal–positive cells (B). (C) Cell morphology and SA-β-gal activity were analyzed by phase-contrast microscopy at day 6 after transfection of 10 nM miR-22 or cont miR. (D) Cell proliferation assay was performed after transfection of 10 nM miR-22, and cells were counted for the indicated days, compared with control cells. Each value was determined in triplicate. **, $P < 0.01$. (E) Cell cycle analysis was performed at 48 h after transfection. The percentage of G1, S, and G2 are demonstrated as shown. The histogram displays the relative changes of G1 and G2 phase compared with S phase. (F) BrdU quantitative analysis was performed at 72 h after transfection, presented by the percentage of BrdU incorporation. (G) Stable expression of miR-22 (Lenti-Pre22) was evaluated by qRT-PCR analysis, presented by the relative quantitation of miR-22 expression level at day 6 after infection. Expression level of miR-22 in Lenti-Pre22–transfected cells was relative to that in Lenti-C–transfected cells set at 1. U6 was used as an internal normalization control. (H) Cell morphology and SA-β-gal activity were analyzed by phase-contrast microscopy at day 6 after infection. The percentage of SA-β-gal–positive cells is presented in the right histogram. (I) Cell proliferation assay was performed at day 6 after infection with Lenti-Pre22 and compared with control cells. Data in all the panels represent mean ± SEM ($n = 3$). *, $P < 0.05$; **, $P < 0.01$. Bars, 50 µm.

Furthermore, silencing of these target genes by siRNAs resulted in growth arrest (Fig. 6 A) and increased SA-β-gal activity in MRC-5 fibroblasts and MDA-D3 cells (Fig. 6 B), as well as morphological changes (not depicted), similar with miR-22–induced senescence phenotypes. We confirmed that the siRNAs against SIRT1 and CDK6 knocked down the expression of SIRT1 and CDK6 and caused dephosphorylation of pRB at ser807/811 (Fig. 6, C and E), which was also induced by either mature miR-22 or premiR-22 overexpression in various different cells (Fig. 6, D and F). In addition,

Published April 18, 2011

A

Gene	GenBank	Conservation	3'UTR Position on mRNA	Binding sites on 3'UTR	Target Site	Prediction algorism
SIRT1	NM_012238	H/P/M/R/D	2298-4089	514-536	3' UGUCAAGAAGUUG--ACCGUCGAA 5'(miR-22) 5' CAUUUUCCAAAACUGU**GGCAGCU**A 3'(UTR)	TargetScan, PicTar, miRanda
SP1	NM_138473	H/P/M/R/D	2456-7656	4719-4741	3' UGUCAAGAAGUUGACCGUCGAA 5'(miR-22) 5' CUACACACACCAGU**GGCAGCU**G 3'(UTR)	TargetScan, PicTar, miRanda
CDK6	NM_001259		1394-11628			
	Site-1	H/P/M/R/D		176-188	3' UGUCAAGAAGUUGACCGUCGAA 5'(miR-22) 5' AAUGCAAGAGUGAUU**GCAGCU**U 3'(UTR)	PicTar
	Site-2	H/P		1862-1884	3' UGUCAAGAAGUUGACCGUCGAA 5'(miR-22) 5' UGUACUGAAUUCUUU**GCAGCU**U 3'(UTR)	PicTar
	Site-3	H/P/D		5928-5950	3' UGUCAAGAAGUUGACCGUCGAA 5'(miR-22) 5' ACAGCACCACAGAAA**GCAGCU**U 3'(UTR)	PicTar

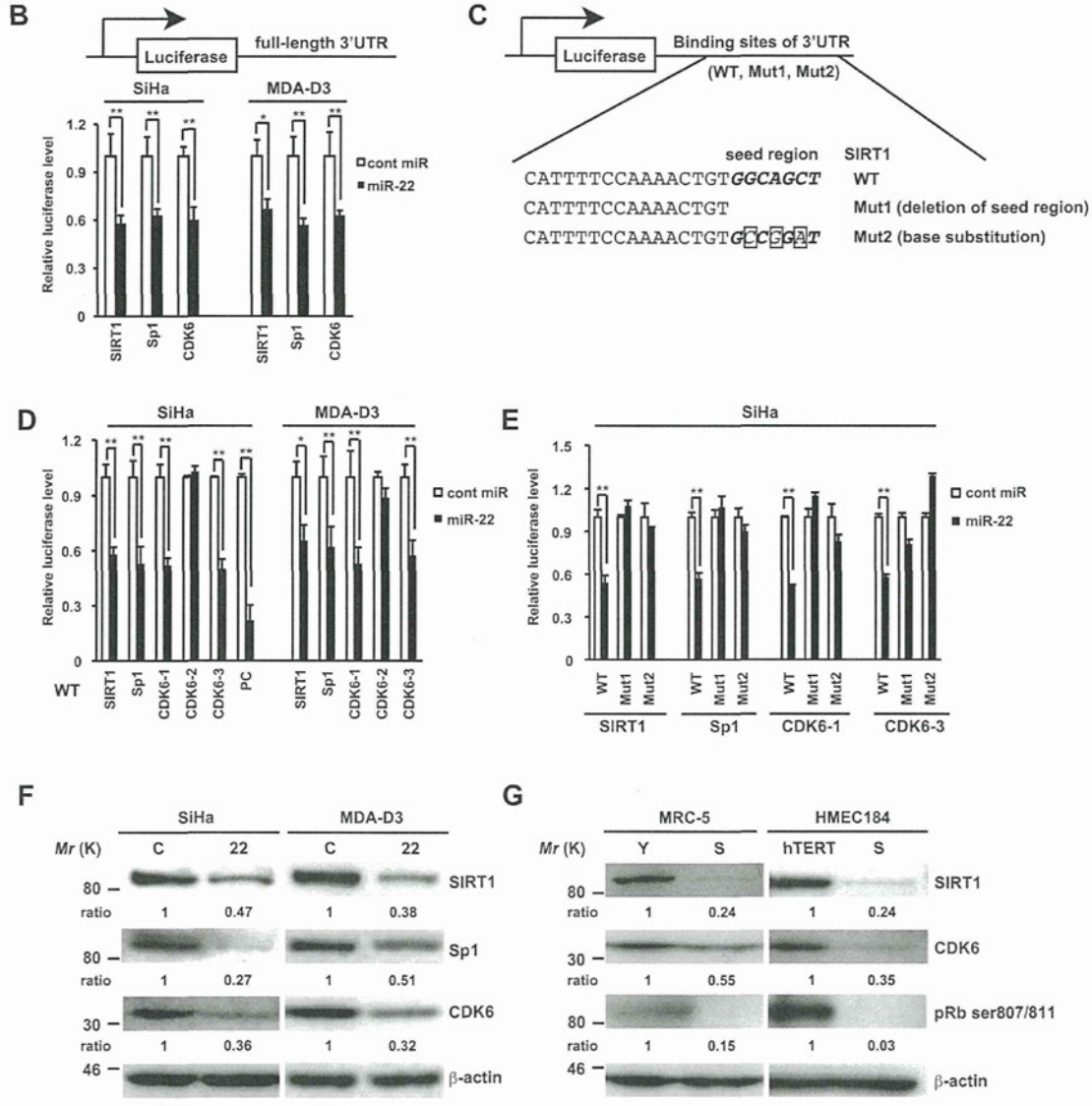

Figure 5. **SIRT1, Sp1, and CDK6 are direct targets of miR-22.** (A) Summary of miR-22 target sites in the 3′-UTR of SIRT1, Sp1, and CDK6. H, human; P, chimp; M, mouse; R, rat; D, dog. The underlined bold nucleotides indicate target sites. (B–E) Target validation of SIRT1, Sp1, and CDK6 was confirmed in the luciferase reporter assay. (C) Scheme of the luciferase reporter constructs containing conserved miR-22 target sites (WT), deletion of seed region (Mut1), or base substitution of seed region (Mut2) was indicated using SIRT1 as an example. The seed region is italic bold, and point mutations are boxed in the seed region. Each construct, including full-length 3′-UTR (B), WT (D), or Muts (E), was cotransfected with miR-22 or cont miR into SiHa or MDA-D3 cells. Relative luciferase level = $(S_{luc}/S_{renilla})/(C_{luc}/C_{renilla})$ in relative light units (RLUs). S_{luc}, RLUs of firefly luciferase activity in miR-22–transfected sample. $S_{renilla}$, RLUs of renilla luciferase activity in miR-22–transfected sample. C_{luc}, RLUs of firefly luciferase activity in cont miR–transfected groups. $C_{renilla}$, RLUs of renilla luciferase

Published April 18, 2011

p53 protein level did not change in MRC-5 and MDA-D3 cells, but p53 expression is up-regulated in miR-22–transfected SiHa cells (Fig. 6 F). These findings indicate that miR-22 may affect the pRb pathway of cellular senescence by targeting SIRT1 and CDK6.

Lastly, we attempted to determine whether overexpression of any of the three genes could rescue the senescence phenotype in cells overexpressing miR-22. We forced SiHa or MDA-D3 cells to express SIRT1, Sp1, or CDK6 using plasmid constructs lacking 3′-UTRs of these genes. Indeed, miR-22–induced cell growth repression and SA-β-gal activity were partially rescued by the introduction of SIRT1, CDK6, or Sp1 in either SiHa cells (Fig. 6, G and H) or MDA-D3 cells (not depicted), although it seemed weak for the effect of Sp1 overexpression on cell growth, which might be because of the indirect role of Sp1 in the pRb pathway of senescence. Collectively, these findings suggest that SIRT1, Sp1, and CDK6 play an important role in miR-22–induced senescence.

miR-22 alters tumor cell morphology and suppresses cell invasiveness in vitro

Changes in cell morphology are important parameters of cancer invasion and metastasis. We performed high content analysis using Operetta to measure the morphology area of all the cells transfected with miR-22, miR-34a, or cont miR on each well of a 96-well plate (Fig. 7 A and Fig. S3 B) and analyzed cell size distribution (Fig. 7 B). We found there were significant differences in cell size distribution between miR-22–treated cells and other cells. miR-22 remarkably increased cell morphology area up to 1.6-fold overall and raised percentages of cells distributed in large cell size groups in comparison with cont miR or miR-34a, revealing that miR-22 triggers senescence morphological changes in tumor cells. In addition, miR-22–treated cells contain enhanced actin stress fibers (Fig. 7 A) similar to senescent fibroblasts, indicating that those cells are less motile (Chen et al., 2000; Belguise et al., 2005). We observed that senescent fibroblasts and Lenti-Pre22–infected cancer cells exhibiting large flattened senescence-like morphology appeared to decrease in cell movement (Fig. S4 and Videos 1–4, large GFP-positive cells), indicating that miR-22–induced senescence morphology in cancer cells could be attributed to the suppression of cell motility. Matrigel invasion assay showed that miR-22 significantly reduced the number of invaded cells in SiHa and MDA-D3 cells (Fig. 7 C), indicating that the invasive potential of cancer cells was severely affected by miR-22. Therefore, the inhibition of cancer cell invasion by miR-22 may be a result of the induction of cellular senescence.

miR-22 inhibits tumor growth and metastatic potential of aggressive breast cancer in vivo

We next asked whether miR-22 overexpression would also induce senescence in vivo and suppress tumor growth and metastasis in vivo. Using breast cancer tumor models, the cont miR–treated mice showed the apparent presence of primary tumor, whereas those injected with miR-22 complex exhibited no increase in the luminescence of primary tumor during the same observation period (Fig. 8 A, left). Judging from photon count between the cont miR– and miR-22–treated groups at the two points of the experiment, miR-22 treatment resulted in a mean decrease in tumor growth of 41.3% at day 39 ($P = 0.04$; not depicted) and 66% at day 46 ($P = 0.005$; Fig. 8 A, right), suggesting that miR-22 exerted significant tumor growth suppression in vivo. We also compared tumor metastasis with important organs in the two groups and were surprised to find that miR-22 delivery resulted in the inhibition of distant metastasis in the liver, kidney, spleen, stomach, and small intestine (Fig. 8 B). There were significant differences in the whole body of mice between the cont miR– and miR-22–treated groups on day 46 ($P = 0.004$), indicating the inhibition of metastasis by injection with miR-22 in vivo.

We also confirmed that synthetic miR-22 was delivered into primary tumor by quantitation of the miR-22 level in tumor (Fig. 8 C). Furthermore, the number of SA-β-gal–positive cells in miR-22–treated tumor dramatically increased, correlated with the amount of miR-22 in tumor (Fig. 8 D). In addition, we did not observe SA-β-gal–positive cells in nontumor cells such as vascular endothelial cells and other stroma cells of mice. Moreover, we found that the morphologies of the tumors were different; the cells in cont miR–treated groups were densely packed and slightly elongated, whereas those in miR-22–treated groups were larger and more irregularly shaped (Fig. 8 E). Pathologically, vacuolation and nuclear pyknosis associated with degradation of tumor cells were found in miR-22–treated tumor tissues. Therefore, it is possible that induction of cellular senescence in tumor cells may result in these pathological changes.

The progression toward metastasis formation requires proliferation of tumor cells at primary sites and distant sites. Notably, the expression of Ki-67 in miR-22–treated groups was significantly lower than that in cont miR–treated groups and nontreated groups (Fig. 8 F), indicating the inhibition of cell proliferation in tumor tissues treated with miR-22. Together, these findings suggest that miR-22 significantly induced cellular senescence in breast cancer in vivo, consequently inhibiting tumor growth and metastasis in vivo.

Discussion

The present study for the first time reported the functional effect of miR-22 as a novel regulator of cellular senescence in normal human and cancer cells and addressed the inhibitory role of miR-22 in tumor growth and metastasis, suggesting that miR-22–induced senescence acts as a barrier to cancer progression in vitro and in vivo. Our study extends the current understanding

activity in cont miR–transfected groups. PC, positive control. (F) Representative Western blot analysis of SIRT1, Sp1, and CDK6 in SiHa and MDA-D3 cells transfected with cont miR (C) and mature miR-22 (22) at 72 h after transfection. (G) The expression levels of SIRT1, CDK6, and pRB phosphorylation in MRC-5 and HMEC184hTERT cells were analyzed by immunoblotting. β-actin was used as a loading control and the relative density of bands was densitometrically quantified. Y, young; S, senescent; hTERT, 184hTERT. Data in all the panels represent mean ± SEM ($n = 3$). *, $P < 0.05$; **, $P < 0.01$.

Published April 18, 2011

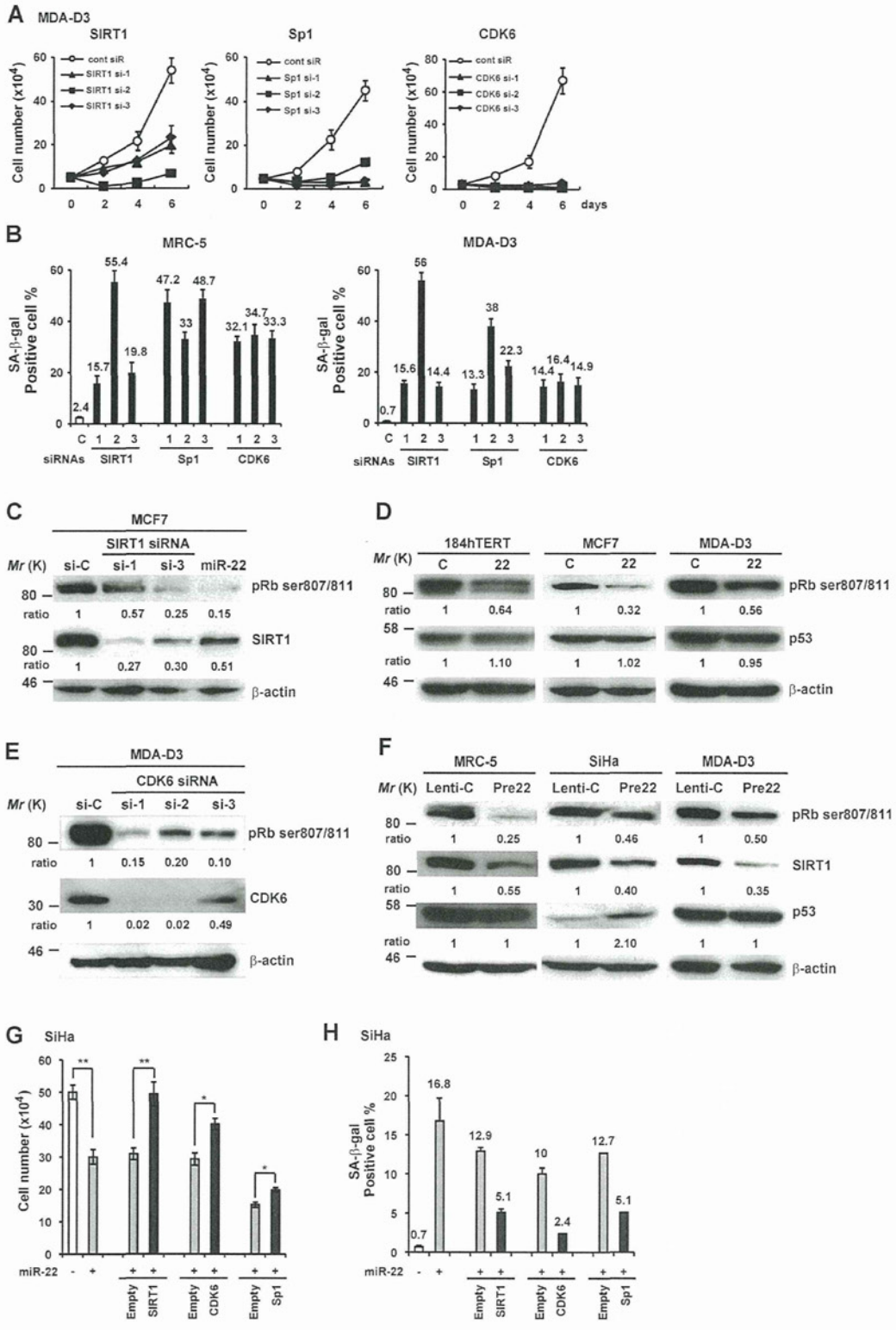

Figure 6. **SIRT1, Sp1, and CDK6 are potentially involved in miR-22–mediated cellular senescence.** (A) Representative growth curves corresponding to MDA-D3 cells transfected with cont siR or siRNAs against SIRT1, Sp1, and CDK6. Each value was determined in triplicate. (B) The histograms display the percentage of SA-β-gal–positive cells in MRC-5 and MDA-D3 cells at day 6 after siRNA transfection. (C–F) Western blot analysis was performed in those cells as indicated in each panel at 72 h after siRNA/miRNA transfection (C–E) or day 6 after infection (F). β-actin was used as a loading control and the relative density of bands was densitometrically quantified. (G and H) SiHa cells were first transfected with miR-22 duplex and, 24 h later, sequentially transfected with expressing plasmids or empty vectors as indicated. Cell proliferation (G) and SA-β-gal (H) activity was evaluated at day 6 after miRNA transfection. Data in all the panels represent mean ± SEM (n = 3). *, $P < 0.05$; **, $P < 0.01$.

Published April 18, 2011

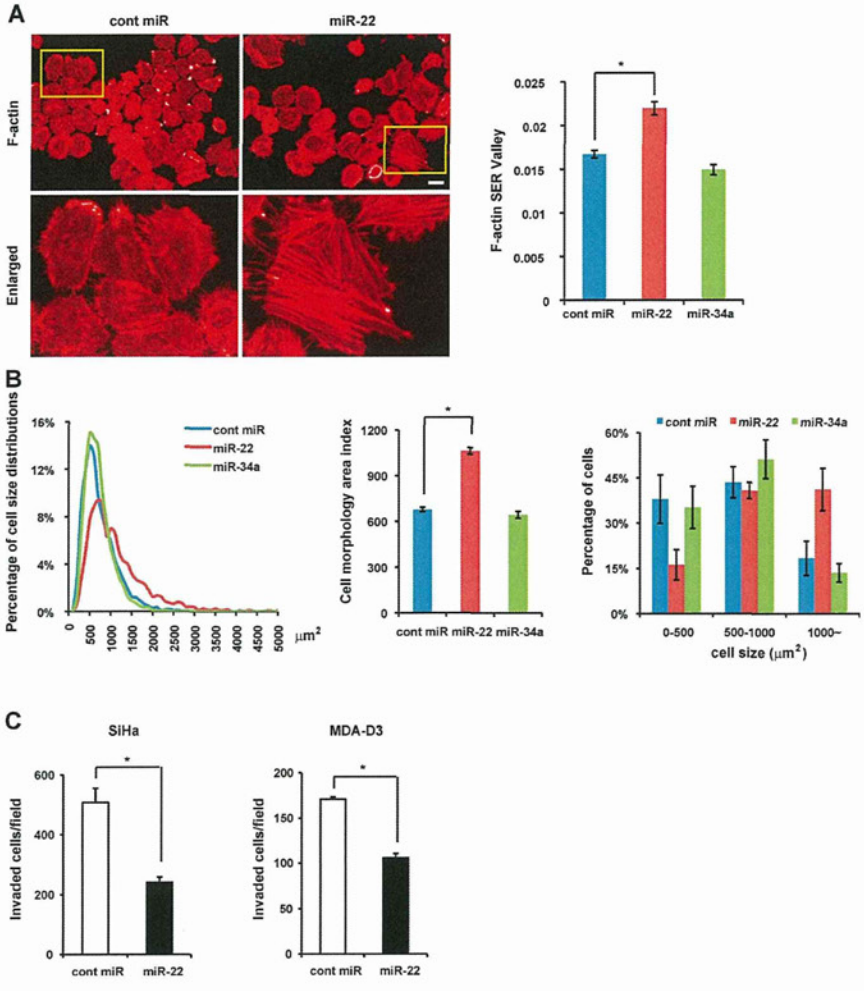

Figure 7. **Overexpression of miR-22 induces cell enlargement and inhibits cell invasion in vitro.** (A) Cell morphology area and actin stress fiber formation (stained with phalloidin) in miR-22–transfected SiHa cells were examined by confocal microscopy and compared with control cells. Enlarged images of the boxed area from the top are shown in the bottom. Bar, 20 μm (top, left and right). The histogram shows that F-actin formation was quantified using the texture analysis, and F-actin SER Valley represented occurrence of stress fiber structures within cells. (B) Cell size distribution (left), overall morphology area (middle), and percentage of cells in three groups of cell size (right) were calculated and analyzed by automated image analysis in SiHa cells. (C) Effect of miR-22 on SiHa and MDA-D3 cell invasion was measured by Matrigel invasion assay for 48 h, presented by quantitative determination of the number of invaded cells. Data in all the panels represent mean ± SEM ($n = 3$). *, $P < 0.05$.

of SA-miRNAs in tumorigenesis by unraveling the role of miR-22 in cellular senescence and tumor suppression. miRNAs present a mechanism in which genes involved in a variety of different signaling pathways can be regulated simultaneously (He and Hannon, 2004; Lafferty-Whyte et al., 2009). Not only does miR-22–induced senescence inhibit unlimited tumor cell proliferation, senescence morphological changes also suppress tumor cell motility and invasion, partially because of enhanced actin stress fibers in cancer cells, indicating that the induction of senescence contributes to the suppression of tumor cell growth, invasion, and metastasis in vitro and in vivo.

Our study shows that miR-22 is differentially expressed in normal human and cancer cells. Consistent with our results, miR-22 dysregulation in cancer and human diseases has been documented in several miRNA profiling experiments. miR-22 is down-regulated in intrahepatic cholangiocarcinoma (Kawahigashi et al., 2009) and silenced in acute lymphoblastic leukemia (Li et al., 2010) and hepatocellular carcinoma (Calin et al., 2004) but up-regulated in osteoarthritis (Iliopoulos et al., 2008). These varying levels of miR-22 expression may suggest different requirements for alterations in their target gene pathways. miR-22 regulates a repertoire of cancer-related genes; however, there is no indication of the importance of miR-22 in tumorigenesis through targeting senescence-associated genes. In the present study, gain-of-function and loss-of-function phenotypes of miR-22 demonstrated the role of miR-22 as a positive regulator of cellular senescence and identified SIRT1, Sp1, and CDK6 as critical targets of miR-22 in the senescence signaling pathway.

Previous studies have documented that SIRT1, Sp1, and CDK6 might act on the p53 and/or pRb pathway. (Ota et al., 2006; Ruas et al., 2007; Tapias et al., 2008; Brooks et al., 2009) SIRT1 plays an important role in the longevity and cellular senescence of most organisms through directly modulating the p16–pRb signaling pathway (Huang et al., 2008) as well as p53 and other proteins (Solomon et al., 2006; Brooks and Gu, 2009). The Sp1 transcription factor regulates the expression of multiple cell cycle genes, including the p53 and Sp1 gene itself (Koutsodontis et al., 2001; Tapias et al., 2008). CDK6 protein has been understood to phosphorylate pRB and delay senescence (Ruas et al., 2007; Ohtani et al., 2009). Our study demonstrated that miR-22 induced the dephosphorylation of pRB by targeting SIRT1 and CDK6. Collectively, we suppose that miR-22 regulates cellular senescence through connecting SIRT1, Sp1, and CDK6 to affect the pRb pathway and might coordinate p53 and other signaling pathways of cellular senescence in a cell type– and genetic context–dependent manner.

Published April 18, 2011

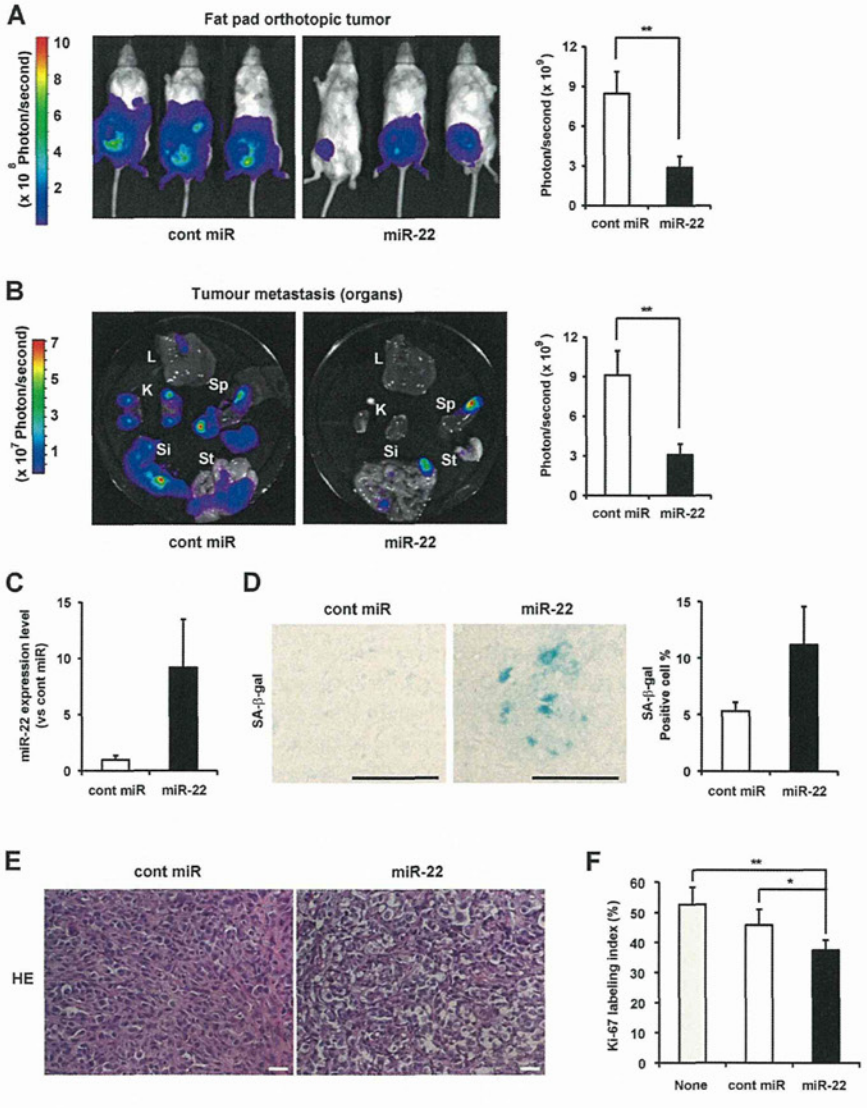

Figure 8. **Synthetic miR-22 delivery induces cellular senescence in vivo and inhibits breast tumor growth and metastasis in vivo.** (A and B) Representative fat pad orthotopic tumor (A) and selected organ (B) images of mice on day 46 after inoculation. Quantitation of bioluminescence emitted from the primary tumor (A) or whole body (B) of mice was presented as the mean ± SEM (n = 6). L, liver; K, kidney; Sp, spleen; Si, small intestine; St, stomach. (C) Relative quantitation of miR-22 level in primary tumor tissues was analyzed by qRT-PCR. Total RNA was isolated from five 10-µm-thick optimal cutting temperature compound–embedded frozen tissue sections. Expression level of miR-22 in miR-22–treated tumors was relative to that in cont miR–treated tumors set at 1. U6 was used as an internal normalization control. Data represent mean ± SEM (n = 5). (D and E) Representative histochemical detection of SA-β-gal activity in vivo (D) and hematoxylin and eosin (HE) staining (E) in primary tumor on day 46 after inoculation. Images were taken with light microscopy. Seven independent fields were chosen, and the percentage of SA-β-gal–positive cells is presented in the histogram. Data represent mean ± SEM (n = 4). Bars, 50 µm. (F) Effect of miR-22 on cell proliferation in primary tumor tissues was evaluated by Ki-67 immunostaining. The histogram displays the percentage of Ki-67 labeling index in these groups. Data represent mean ± SEM (n = 3). *, $P < 0.05$; **, $P < 0.01$.

The ability of miRNAs to affect many mRNAs is similar to the ability of transcription factors to regulate many promoters simultaneously. Recent studies demonstrate that miR-22 constitutes a feedback loop with c-myc and MYCBP and forms a regulatory loop in the phosphatase and tensin homolog–AKT pathway (Iliopoulos et al., 2008; Pandey and Picard, 2009; Bar and Dikstein, 2010; Xiong et al., 2010). The human miR-22 gene is located in a minimal loss of heterozygosity region on chromosome 17 close to p53 (Calin et al., 2004). We predict that miR-22 might induce complex changes and the extensive cooperation between miR-22 and p53 known to be involved in the senescence program, which remains to be elucidated.

miR-22 has been shown to be ubiquitously expressed in human cells and various tissues (Neely et al., 2006). Expression of miR-22 increases after the induction of stem cell differentiation and in erythropoiesis, which indicates that it might have an important role in cell development and differentiation (Choong et al., 2007; Gangaraju and Lin, 2009). miR-22 is highly expressed in mammary progenitor cells, implicating its possible role in progenitor self-renewal (Ibarra et al., 2007). To date, there is no indication of miR-22 function in normal human cells. In our study, miR-22 is particularly up-regulated upon cellular senescence in human fibroblasts and epithelial cells, and overexpression of miR-22 induced senescence phenotypes in these cells, indicating that miR-22 might emerge as the principal regulator that controls cell functions in physiological and pathophysiological settings. However, it is obscure in the mechanism that controls the increased expression of miR-22 during senescence. We attempted stable knockdown of miR-22 in early-passage MRC-5 (Fig. 2 D) and IMR90 cells (unpublished data), which resulted in both of the cells seeming younger than untreated cells. Furthermore, we investigated how stable knockdown of miR-22 affected late-passage MRC-5 cells. Our results demonstrated that those anti-22–infected presenescent MRC-5 cells appeared to be small, thin, and young with the decrease in cell morphology area and fewer SA-β-gal–positive cells (Fig. 2, C–F), indicating that inhibition of miR-22 is an obstacle for cells to undergo senescence. Given our finding that miR-22 induces cellular senescence in human fibroblasts in vitro, it will be interesting to determine whether miR-22 is involved in human aging in vivo.

Published April 18, 2011

It has been reported that the regulation of proliferation signaling, cytoskeletal remodeling, and apoptosis survival pathways would logically be required to create the senescent cell phenotype, which can be regulated by SA-miRNAs with differential timings of these complex signaling cascades (Lafferty-Whyte et al., 2009). These might give an explanation to the distinct effects of miR-22 knockdown on cell proliferation, morphology, and viability in various cells. We observed that actin stress fibers were enhanced in miR-22–transfected enlarged cells (Fig. 7 A), whereas anti-22–infected cells appeared to be small and to have fewer stress fibers (unpublished data). Moreover, we noted that cytoskeleton arrangement and focal adhesion turnover occurred with differential timing in various anti-22–infected cells and thus might affect cell growth, adhesion, and survival, which needs to be confirmed in a further study. In addition, miR-22 expression level is quite low in various cancer cells, and permanent inhibition of miR-22 induced apoptosis, indicating that miR-22 kept to a certain level seems to be essential for cellular survival. It has been reported that miR-22 targets the phosphatase and tensin homolog and anti-22 induces apoptosis in different cancer cells (Bar and Dikstein, 2010; Liu et al., 2010), which is consistent with our results.

In this study, miR-22 inhibits the proliferation of human breast cancer metastasis cell lines (MDA-D3) both in vitro and in vivo through induction of genetic reprogramming of the senescent pathway. Synthetic miR-22 injection significantly suppresses tumor growth and metastasis in a mouse model of breast cancer metastasis, indicating the therapeutic potential of miR-22 in breast cancer metastasis. Currently, the emergence of new technologies that use synthetic miRNA mimics or anti–miRNA oligonucleotides holds great promise in clinical miRNA therapy (Garofalo and Croce, 2011). The first clinical trial for LNA-antimiR-122–based hepatitis C therapeutics was initiated after the successful therapeutic application of miR-122 antagonism in mice (Elmén et al., 2008), whereas the clinical application of synthetic miRNA mimics has not been reported. Synthetic miR-22 mimic treatment in cancer will become a significant scientific and therapeutic challenge.

SA-miRNAs, such as miR-22, induce cellular senescence without causing apoptosis in cancer cells and subsequently result in tumor suppression (Fig. S5), providing a novel promising approach for the next generation of cancer therapy using nucleic acid biomedicine. We propose that permanent micromanaging of cancer cells by inducing senescence phenotypes using SA-miRNAs may be novel and efficient for protecting recurrent cancer after conventional cancer treatments without causing side effects.

Materials and methods

Cell culture

MRC-5 cells were grown in DME/F12 (1:1, vol/vol) supplemented with SAP (0.2 mM serine, 0.1 mM aspartic acid, and 1.0 mM pyruvate). MDA-MB-231-luc-D3H2LN is a luciferase-expressing cell line that was derived from MDA-MB-231 cells, maintained in RPMI1640 medium. Other human fibroblasts and cancer cells were cultured in DME. All media were supplemented with 10% FBS (vol/vol). HMEC184 cells were cultured in MEGM BulletKit (Takara Bio Inc.). TIG-3 (74–76 PDL), TIG-1 (63 PDL), TIG-114 (51 PDL), MRC-5 (58–60 PDL), and HMEC184 (22 PDL) were cultured for 2–4 wk as senescent normal cells. MRC-5 (41–51 PDL) and 184hTERT (84–100 PDL) were used as young fibroblasts and immortalized epithelial cells, respectively.

miRNA microarray

Total RNAs were harvested from young (42 PDL) and senescent (74 PDL) TIG-3 fibroblasts using the traditional acid guanidinium-phenol-chloroform extraction method and quantified with a spectrophotometer (NanoDrop; Thermo Fisher Scientific). Microarray analysis of miRNA expression was performed by both miRCURY LNA miRNA Array (Exiqon) and 3D-Gene microarray (Toray).

Real-time qPCR

Total RNA was extracted from the cells and tissues using the miRNeasy Mini kit (QIAGEN). The expression of miRNA was quantified by miRNA assays (TaqMan; Applied Biosystems). Real-time qRT-PCR was performed using a real-time PCR system (ABI StepOne and StepOnePlus; Applied Biosystems) and LightCycle 480 (Roche). Expression of miRNA was defined from the threshold cycle, and relative expression levels were calculated using the $2^{-\Delta\Delta Ct}$ method after normalization with reference to the expression of U6 small nuclear RNA.

Transient miRNA/siRNA transfection and plasmid transfection

Hsa-miR-22 duplex and negative control were obtained from QIAGEN. siRNAs targeting SIRT1, Sp1, CDK6, and negative control siRNA were purchased from Invitrogen. Cells were transfected with 10 nM of either miRNA or siRNA (except as mentioned) using Lipofectamine RNAiMax (Invitrogen) according to the manufacturer's protocol. Transfection efficiency under the conditions we adopted in this study was estimated to be >90% according to our observations made using a fluorescence-labeled double-stranded siRNA.

For rescue experiments, the expression plasmids used were pcDNA3.1-SIRT1 (a gift from B. Marshall, Gladstone Institute, San Francisco, CA), pCMVneo-CDK6 (provided by S. Van den Heuvel, Utrecht University, Utrecht, Netherlands), and CMV-Sp1 (Addgene). These constructs contain the encoding region of mRNA but lack the 3′-UTR of these genes. Cells were first transfected with miRNA in a 60-mm dish for 24 h and sequentially transfected with 0.25 µg of plasmid DNA using Lipofectamine LTX Plus reagent (Invitrogen) according to the manufacturer's protocol. The overexpression of SIRT1, Sp1, and CDK6 was confirmed by Western blotting. After a 24-h incubation, cells were seeded to 35-mm-diameter dishes and incubated for 4 d until cell proliferation assay and SA-β-gal assay.

Lentivirus infection

Lentiviruses were generated by cotransfecting 0.9 µg of lentiviral vector (premiR-22, miRZip, anti–miR-22, or empty vectors; System Biosciences) and 2.7 µg of packaging plasmid mix (1:1:1 for 0.9 µg pPACK-H1-GAG, pPACK-H1-Rev, and pVSV-G) in 293T cells using Lipofectamine LTX Plus reagent. Supernatants were collected 48 h after transfection, filtered through a 0.45-µm membrane, and directly used to infect cells. Cells were observed and images were acquired using a 10× objective with fluorescent microscopy (Axiovert 200M; Carl Zeiss) in combination with a camera (AxioCam; Carl Zeiss) and AxioVision software (Carl Zeiss) at room temperature.

Cell proliferation and SA-β-gal assay

For cell proliferation assay, 48 h after transfection or infection, 3–5 × 10^4 cells were seeded in a series of 35-mm-diameter dishes and counted for the indicated days. For cytochemical and histochemical detection of SA-β-gal activity, SA-β-gal staining was performed as described previously (Debacq-Chainiaux et al., 2009). SA-β-gal–positive cells were quantified by counting positive and negative cells at 100× magnification in at least five random independent fields. Pictures were taken with a 10× phase-contrast objective on a light microscope (IMT-2; Olympus) with a camera using Image saver (AE-6905; ATTO) at room temperature.

Automated image acquisition

SiHa cells were seeded in a 96-well Viewplate (PerkinElmer) and transfected with cont miR, miR-22, or miR-34a for 72 h. To measure cell size and F-actin, cells were fixed by 4% PFA and stained with the actin marker Rhodamine phalloidin (1:40; Invitrogen; provided by S. Kobayashi and H. Kishi, Yamaguchi University, Ube, Japan). For BrdU quantitative analysis, cells were pulse labeled with 10 µM BrdU (Sigma-Aldrich) for 1 h at 37°C, incubated with 5% CO_2, and fixed by 70% ice-cold ethanol for 30 min at room temperature. Cells were treated with 2N HCl for 20 min, neutralized with 0.2 M Tris-HCl, pH 7.5, and permeabilized with 0.1% Triton X-100 for 5 min, followed by the mouse anti-BrdU (1:200; Dako) and incubation for

Published April 18, 2011

1 h. Cells were then stained with anti–mouse AF488 (1:500; Invitrogen). DAPI (1 µg/ml; Dojindo) images were used for nuclear recognition and cell counting. Images were acquired in a fully automated and unbiased manner using a 10× objective with a spinning disk confocal microscope (Operetta; PerkinElmer) at room temperature. Eight images per well were collected to obtain a sufficient number of cells for reliable statistical analysis. Image correction and analysis were performed using custom-designed image analysis software (Harmony; PerkinElmer). The histogram in Fig. 7 A shows that F-actin was quantified using the texture analysis by Harmony software (PerkinElmer), and F-actin SER Valley represented the occurrence of stress fiber structures within cells.

FACS analysis
48 h after transfection, cells were fixed in 70% ice-cold ethanol and stained with PBS containing 50 µg/ml propidium iodide and 100 µg/ml RNase A for DNA content analysis by flow cytometry analysis on a FACSCalibur system (BD). The percentage of cells in the various cell cycle phases was calculated using ModFitLT v2.0 software (Verity Software House).

Apoptosis assays
Cells were plated in an 8-well CultureSlide (BD), and apoptotic cells were detected with traditional or modified TUNEL assay using the DeadEnd Fluorometric TUNEL System (Promega) according to the manufacturer's protocol. In modified TUNEL assay, Cy5-dUTP (GE Healthcare) was substituted for fluorescein-dUTP in a standard TUNEL reaction to detect apoptotic cells of GFP-expressed cells. Images were acquired using a 40× objective with fluorescent microscopy (Axiovert 200M) in combination with a camera (AxioCam) and AxioVision software at room temperature.

Hybridization protection assay (HPA) and Southern blot analysis
Cells were plated in a 100-mm culture dish and transfected, and DNA was extracted with a traditional phenol-chloroform 72 h after transfection. The lengths of total telomere and G-tail were determined using Southern blotting and HPA methods as described previously (Tahara et al., 2005).

Western blotting
72 h after transfection or at day 6 after infection, cells were homogenized in lysis buffer (50 mM Tris-HCl, pH 8.0, 120 mM NaCl, 1% NP-40, 100 mM NaF, 0.2 mM Na_3VO_4, and Complete mini protein inhibitor cocktail [Roche]). 30 µg of proteins in the total cell lysate was separated by SDS-PAGE and transferred to polyvinylidene fluoride membrane. Antibodies to p53 (clone BP53-12; Millipore), phospho-Rb (ser807/811; Cell Signaling Technology), and β-actin (Sigma-Aldrich) were purchased, and anti-CDK6 (C-21), SIRT1 (H-300), and Sp1 (PEP2) antibodies were purchased from Santa Cruz Biotechnology, Inc. The secondary antibodies were HRP-conjugated anti–rabbit (NA 934V) and –mouse (NA 931V) antibodies (GE Healthcare). Immunoreactive bands were visualized using an ECL Plus kit (GE Healthcare), followed by exposure to x-ray film (RX-U; Fujifilm). The density of bands was densitometrically quantified using ImageJ (National Institutes of Health).

Luciferase reporter assay
The full-length 3′-UTRs of human SIRT1 and Sp1 were amplified by PCR from genomic DNA and cloned at the SacI and XhoI sites into pmirGLO vector (Promega). The 3′-UTR fragments of human CDK6 containing three putative miR-22 binding sites were also amplified from genomic DNA and cloned at the XhoI and SalI sites into pmirGLO vector. The sense and antisense oligonucleotides for the putative miR-22 binding site at the 3′-UTR of potential targets were annealed and cloned at the SacI and XbaI sites into pmirGLO vector. An internal NotI site was added to the oligonucleotides for clone confirmation. A positive control construct contains complete complementary mature miR-22 sequence. PCR primers and oligonucleotide sequences for constructs are provided in Table S2. All the constructs were further confirmed by sequencing.

For luciferase activity analysis, each construct was cotransfected with miRNA duplex in a 96-well plate using DharmFECT Duo transfection reagent (Thermo Fisher Scientific) for 72 h, and luciferase assays were performed with the Dual-Luciferase reporter system (Promega) according to the manufacturer's instructions. Luminescent signal was quantified by luminometer (Glomax; Promega), and each value from firefly luciferase construct was normalized by Renilla luciferase assay.

Cell motility observation by fluorescence microscopy
Cells were seeded in a 4-well 35-mm dish (Greiner Bio-One) at a density of 1,000 cells/well and grown for 48 h in culture medium. Before recordings were initiated, the multidishes were left for at least 30 min on the microscope stage for temperature equilibration. Time-laspe video recordings of live cells were performed for determination of cell motility. In brief, live cells from several nonoverlapping areas were recorded in 30-min or 1-h intervals over a period of 8–24 h using a CFI Plan Apo 10× objective with a fluorescence microscope (BIOREVO BZ-9000; KEYENCE) equipped with a motorized movable microscope stage. Recordings were stored as 8-bit 680 × 512 pixel images. The microscope stage contained a thermostatically controlled heating element and was surrounded by a Plexiglas incubator, thereby ensuring that live specimens could be maintained at 37°C during recordings.

In vitro invasion assay
48 h after transfection, cells were resuspended in culture medium without serum and seeded at densities of 1.5×10^5 cells/well in 24-well Transwell inserts (8-µm pores; BD) coated with 50 µg Matrigel (BD). The lower chamber was supplemented with a medium with 10% FBS. After 48 h of incubation, the cells on the upper surface were scraped off, whereas the invasive cells attached to the lower surface of the membrane inserts were fixed and stained with hematoxylin. The invading cells were observed and counted from nine images (including at least 2,000 cells) in three fields of three membranes using a 10× phase-contrast objective under light microscopy (U-PMTVC; Olympus) at room temperature.

Tumor imaging in vivo
5-wk-old female C.B17/Icr-scid (Scid/scid) mice (CLEA Japan, Inc.) were inoculated with MDA-MB-231-luc-D3H2LN cells into the fat pad on day 0 as a 1:1 mixture of ECM gel complex and cells at 2×10^6 cells/50 µl/site. The hsa-miR-22 duplex and cont miR with RNA-jetPEI (Polyplus Transfection) complex at the ratio of 1:1 in a volume of 100 µl (20 µg/site) were injected intratumorally every other day from day 13 to 31 after inoculation. The development of subsequent tumor growth and metastasis was monitored once a week by in vivo imaging. In brief, mice were injected with 150 mg/kg D-luciferin (Promega) intraperitoneally and imaged immediately to count the photons from the whole bodies using the IVIS imaging system (Xenogen) according to the manufacturer's instructions. 10 min later, photons from firefly luciferase were counted. Data were analyzed using LivingImage software (version 2.5; Xenogen).

Immunohistochemistry
Immunohistochemical staining was performed with anti–Ki-67 monoclonal antibody (1:50; Dako) after antigen retrieval by microwave treatment in citrate buffer, pH 6.0, and detection by a streptavidin–biotin peroxidase system using the LSAB kit (Dako). The sections were incubated with primary antibody at 4°C overnight. A labeling index percentage of Ki-67 was determined by examining at least 500 tumor cells at 200× magnification in three representative and intensely stained areas using a 20× objective under light microscopy (U-PMTVC) at room temperature. The expression of Ki-67 was graded as high (>50% of positive cells) and low (<50% of positive cells).

Statistical analysis
Significance of differences between the treated samples and controls was determined by two-tailed *t* tests using Excel (Microsoft). $P < 0.05$ was considered statistically significant.

Online supplemental material
Fig. S1 shows the opposite effect of miR-22 overexpression and knockdown on apoptosis in human cancer cells. Fig. S2 shows that miR-22 has no effect on the length of total telomere or G-tail in human cancer cells. Fig. S3 shows an examination of BrdU quantity analysis, cell morphology area, and F-actin formation by automated image analysis. Fig. S4 shows the images of cell motility observation in senescent fibroblasts and Lenti-Pre22–infected MDA-D3 cells. Fig. S5 shows a scheme for the role of miR-22–induced senescence in cancer cells. Table S1 shows altered expression miRNAs identified by miRNA microarray function in cell growth and tumorigenesis. Table S2 shows PCR primers and oligonucleotide sequences for each construct of miR-22 putative targets in luciferase reporter assay. Videos 1–4 show cell motility observation of young and senescent MRC-5 cells, Lenti-C, and Lenti-Pre22–infected MDA-D3 cells, respectively. Online supplemental material is available at http://www.jcb.org/cgi/content/full/jcb.201010100/DC1.

We thank Maki Yoshida for her assistance with the invasion assay experiments, Ryo Shioda (PerkinElmer, Japan) for his technical help with automated image acquisition, Sei Kobayashi and Hiroko Kishi (Yamaguchi University) for the provided reagents, and Anno Kumiko (Hiroshima University) and Takayuki Mizutani (IZM, Inc., Japan) for their technical support.

Published April 18, 2011

This work was supported by the Grant-in-Aid for Scientific Support Programs for Cancer Research; Grant-in-Aid for Scientific Research on Innovative Areas; and Ministry of Education, Culture, Sports, Science, and Technology of Japan (H. Tahara). This work was partially supported by the Science and Technology Incubation Program in Advanced Regions, Japan Science and Technology Agency, and Takeda Science Foundation (H. Tarara) and the Program for the Promotion of Fundamental Studies in Health Science of the National Institute of Biomedical Innovation (T. Ochiya).

Submitted: 20 October 2010
Accepted: 18 March 2011

References

Adams, P.D. 2007. Remodeling of chromatin structure in senescent cells and its potential impact on tumor suppression and aging. *Gene.* 397:84–93. doi:10.1016/j.gene.2007.04.020

Agirre, X., A. Jiménez-Velasco, E. San José-Enériz, L. Garate, E. Bandrés, L. Cordeu, O. Aparicio, B. Saez, G. Navarro, A. Vilas-Zornoza, et al. 2008. Down-regulation of hsa-miR-10a in chronic myeloid leukemia CD34+ cells increases USF2-mediated cell growth. *Mol. Cancer Res.* 6:1830–1840. doi:10.1158/1541-7786.MCR-08-0167

Akao, Y., Y. Nakagawa, and T. Naoe. 2006. let-7 microRNA functions as a potential growth suppressor in human colon cancer cells. *Biol. Pharm. Bull.* 29:903–906. doi:10.1248/bpb.29.903

Bar, N., and R. Dikstein. 2010. miR-22 forms a regulatory loop in PTEN/AKT pathway and modulates signaling kinetics. *PLoS ONE.* 5:e10859. doi:10.1371/journal.pone.0010859

Bartel, D.P. 2004. MicroRNAs: genomics, biogenesis, mechanism, and function. *Cell.* 116:281–297. doi:10.1016/S0092-8674(04)00045-5

Belguise, K., N. Kersual, F. Galtier, and D. Chalbos. 2005. FRA-1 expression level regulates proliferation and invasiveness of breast cancer cells. *Oncogene.* 24:1434–1444. doi:10.1038/sj.onc.1208312

Braig, M., S. Lee, C. Loddenkemper, C. Rudolph, A.H. Peters, B. Schlegelberger, H. Stein, B. Dörken, T. Jenuwein, and C.A. Schmitt. 2005. Oncogene-induced senescence as an initial barrier in lymphoma development. *Nature.* 436:660–665. doi:10.1038/nature03841

Brooks, C.L., and W. Gu. 2009. How does SIRT1 affect metabolism, senescence and cancer? *Nat. Rev. Cancer.* 9:123–128. doi:10.1038/nrc2562

Calin, G.A., and C.M. Croce. 2006. MicroRNA signatures in human cancers. *Nat. Rev. Cancer.* 6:857–866. doi:10.1038/nrc1997

Calin, G.A., C. Sevignani, C.D. Dumitru, T. Hyslop, E. Noch, S. Yendamuri, M. Shimizu, S. Rattan, F. Bullrich, M. Negrini, and C.M. Croce. 2004. Human microRNA genes are frequently located at fragile sites and genomic regions involved in cancers. *Proc. Natl. Acad. Sci. USA.* 101:2999–3004. doi:10.1073/pnas.0307323101

Campisi, J. 2005. Senescent cells, tumor suppression, and organismal aging: good citizens, bad neighbors. *Cell.* 120:513–522. doi:10.1016/j.cell.2005.02.003

Chen, Q.M., V.C. Tu, J. Catania, M. Burton, O. Toussaint, and T. Dilley. 2000. Involvement of Rb family proteins, focal adhesion proteins and protein synthesis in senescent morphogenesis induced by hydrogen peroxide. *J. Cell Sci.* 113:4087–4097.

Chen, Y., Y. Song, Z. Wang, Z. Yue, H. Xu, C. Xing, and Z. Liu. 2010. Altered expression of MiR-148a and MiR-152 in gastrointestinal cancers and its clinical significance. *J. Gastrointest. Surg.* 14:1170–1179. doi:10.1007/s11605-010-1202-2

Choong, M.L., H.H. Yang, and I. McNiece. 2007. MicroRNA expression profiling during human cord blood-derived CD34 cell erythropoiesis. *Exp. Hematol.* 35:551–564. doi:10.1016/j.exphem.2006.12.002

Collado, M., J. Gil, A. Efeyan, C. Guerra, A.J. Schuhmacher, M. Barradas, A. Benguría, A. Zaballos, J.M. Flores, M. Barbacid, et al. 2005. Tumour biology: senescence in premalignant tumours. *Nature.* 436:642. doi:10.1038/436642a

Debacq-Chainiaux, F., J.D. Erusalimsky, J. Campisi, and O. Toussaint. 2009. Protocols to detect senescence-associated beta-galactosidase (SA-betagal) activity, a biomarker of senescent cells in culture and in vivo. *Nat. Protoc.* 4:1798–1806. doi:10.1038/nprot.2009.191

Deng, Y., S.S. Chan, and S. Chang. 2008. Telomere dysfunction and tumour suppression: the senescence connection. *Nat. Rev. Cancer.* 8:450–458. doi:10.1038/nrc2393

Díaz, R., J. Silva, J.M. García, Y. Lorenzo, V. García, C. Peña, R. Rodríguez, C. Muñoz, F. García, F. Bonilla, and G. Domínguez. 2008. Deregulated expression of miR-106a predicts survival in human colon cancer patients. *Genes Chromosomes Cancer.* 47:794–802. doi:10.1002/gcc.20580

Dimri, G.P., X. Lee, G. Basile, M. Acosta, G. Scott, C. Roskelley, E.E. Medrano, M. Linskens, I. Rubelj, O. Pereira-Smith, et al. 1995. A biomarker that identifies senescent human cells in culture and in aging skin in vivo. *Proc. Natl. Acad. Sci. USA.* 92:9363–9367. doi:10.1073/pnas.92.20.9363

Elmén, J., M. Lindow, A. Silahtaroglu, M. Bak, M. Christensen, A. Lind-Thomsen, M. Hedtjärn, J.B. Hansen, H.F. Hansen, E.M. Straarup, et al. 2008. Antagonism of microRNA-122 in mice by systemically administered LNA-antimiR leads to up-regulation of a large set of predicted target mRNAs in the liver. *Nucleic Acids Res.* 36:1153–1162. doi:10.1093/nar/gkm1113

Fabbri, M., R. Garzon, A. Cimmino, Z. Liu, N. Zanesi, E. Callegari, S. Liu, H. Alder, S. Costinean, C. Fernandez-Cymering, et al. 2007. MicroRNA-29 family reverts aberrant methylation in lung cancer by targeting DNA methyltransferases 3A and 3B. *Proc. Natl. Acad. Sci. USA.* 104:15805–15810. doi:10.1073/pnas.0707628104

Gangaraju, V.K., and H. Lin. 2009. MicroRNAs: key regulators of stem cells. *Nat. Rev. Mol. Cell Biol.* 10:116–125. doi:10.1038/nrm2621

Garofalo, M., and C.M. Croce. 2011. microRNAs: Master regulators as potential therapeutics in cancer. *Annu. Rev. Pharmacol. Toxicol.* 51:25–43. doi:10.1146/annurev-pharmtox-010510-100517

Haferkamp, S., S.L. Tran, T.M. Becker, L.L. Scurr, R.F. Kefford, and H. Rizos. 2009. The relative contributions of the p53 and pRb pathways in oncogene-induced melanocyte senescence. *Aging (Albany NY).* 1:542–556.

Hahn, W.C., and R.A. Weinberg. 2002. Rules for making human tumor cells. *N. Engl. J. Med.* 347:1593–1603. doi:10.1056/NEJMra021902

He, L., and G.J. Hannon. 2004. MicroRNAs: small RNAs with a big role in gene regulation. *Nat. Rev. Genet.* 5:522–531. doi:10.1038/nrg1379

Huang, J., Q. Gan, L. Han, J. Li, H. Zhang, Y. Sun, Z. Zhang, and T. Tong. 2008. SIRT1 overexpression antagonizes cellular senescence with activated ERK/S6k1 signaling in human diploid fibroblasts. *PLoS ONE.* 3:e1710.

Hummel, R., D.J. Hussey, and J. Haier. 2010. MicroRNAs: predictors and modifiers of chemo- and radiotherapy in different tumour types. *Eur. J. Cancer.* 46:298–311. doi:10.1016/j.ejca.2009.10.027

Ibarra, I., Y. Erlich, S.K. Muthuswamy, R. Sachidanandam, and G.J. Hannon. 2007. A role for microRNAs in maintenance of mouse mammary epithelial progenitor cells. *Genes Dev.* 21:3238–3243. doi:10.1101/gad.1616307

Iliopoulos, D., K.N. Malizos, P. Oikonomou, and A. Tsezou. 2008. Integrative microRNA and proteomic approaches identify novel osteoarthritis genes and their collaborative metabolic and inflammatory networks. *PLoS ONE.* 3:e3740. doi:10.1371/journal.pone.0003740

Jessel, R., S. Haertel, C. Socaciu, S. Tykhonova, and H.A. Diehl. 2002. Kinetics of apoptotic markers in exogeneously induced apoptosis of EL4 cells. *J. Cell. Mol. Med.* 6:82–92. doi:10.1111/j.1582-4934.2002.tb00313.x

Katakowski, M., X. Zheng, F. Jiang, T. Rogers, A. Szalad, and M. Chopp. 2010. MiR-146b-5p suppresses EGFR expression and reduces in vitro migration and invasion of glioma. *Cancer Invest.* 28:1024–1030. doi:10.3109/07357907.2010.512596

Kawahigashi, Y., T. Mishima, Y. Mizuguchi, Y. Arima, S. Yokomuro, T. Kanda, O. Ishibashi, H. Yoshida, T. Tajiri, and T. Takizawa. 2009. MicroRNA profiling of human intrahepatic cholangiocarcinoma cell lines reveals biliary epithelial cell-specific microRNAs. *J. Nippon Med. Sch.* 76:188–197. doi:10.1272/jnms.76.188

Kong, W., L. He, M. Coppola, J. Guo, N.N. Esposito, D. Coppola, and J.Q. Cheng. 2010. MicroRNA-155 regulates cell survival, growth, and chemosensitivity by targeting FOXO3a in breast cancer. *J. Biol. Chem.* 285:17869–17879. doi:10.1074/jbc.M110.101055

Kota, J., R.R. Chivukula, K.A. O'Donnell, E.A. Wentzel, C.L. Montgomery, H.W. Hwang, T.C. Chang, P. Vivekanandan, M. Torbenson, K.R. Clark, et al. 2009. Therapeutic microRNA delivery suppresses tumorigenesis in a murine liver cancer model. *Cell.* 137:1005–1017. doi:10.1016/j.cell.2009.04.021

Koutsodontis, G., I. Tentes, P. Papakosta, A. Moustakas, and D. Kardassis. 2001. Sp1 plays a critical role in the transcriptional activation of the human cyclin-dependent kinase inhibitor p21(WAF1/Cip1) gene by the p53 tumor suppressor protein. *J. Biol. Chem.* 276:29116–29125. doi:10.1074/jbc.M104130200

Lafferty-Whyte, K., C.J. Cairney, N.B. Jamieson, K.A. Oien, and W.N. Keith. 2009. Pathway analysis of senescence-associated miRNA targets reveals common processes to different senescence induction mechanisms. *Biochim. Biophys. Acta.* 1792:341–352.

Lee, Y.S., and A. Dutta. 2007. The tumor suppressor microRNA let-7 represses the HMGA2 oncogene. *Genes Dev.* 21:1025–1030. doi:10.1101/gad.1540407

Li, N., H. Fu, Y. Tie, Z. Hu, W. Kong, Y. Wu, and X. Zheng. 2009. miR-34a inhibits migration and invasion by down-regulation of c-Met expression in human hepatocellular carcinoma cells. *Cancer Lett.* 275:44–53. doi:10.1016/j.canlet.2008.09.035

Li, X., J. Liu, R. Zhou, S. Huang, S. Huang, and X.M. Chen. 2010. Gene silencing of MIR22 in acute lymphoblastic leukaemia involves histone modifications independent of promoter DNA methylation. *Br. J. Haematol.* 148:69–79. doi:10.1111/j.1365-2141.2009.07920.x

Liu, L., Y. Jiang, H. Zhang, A.R. Greenlee, R. Yu, and Q. Yang. 2010. miR-22 functions as a micro-oncogene in transformed human bronchial epithelial cells induced by anti-benzo[a]pyrene-7,8-diol-9,10-epoxide. *Toxicol. In Vitro.* 24:1168–1175. doi:10.1016/j.tiv.2010.02.016

Liu, Q., H. Fu, F. Sun, H. Zhang, Y. Tie, J. Zhu, R. Xing, Z. Sun, and X. Zheng. 2008. miR-16 family induces cell cycle arrest by regulating multiple cell cycle genes. *Nucleic Acids Res.* 36:5391–5404. doi:10.1093/nar/gkn522

Narita, M., and S.W. Lowe. 2005. Senescence comes of age. *Nat. Med.* 11:920–922. doi:10.1038/nm0905-920

Narita, M., S. Nũnez, E. Heard, M. Narita, A.W. Lin, S.A. Hearn, D.L. Spector, G.J. Hannon, and S.W. Lowe. 2003. Rb-mediated heterochromatin formation and silencing of E2F target genes during cellular senescence. *Cell.* 113:703–716. doi:10.1016/S0092-8674(03)00401-X

Neely, L.A., S. Patel, J. Garver, M. Gallo, M. Hackett, S. McLaughlin, M. Nadel, J. Harris, S. Gullans, and J. Rooke. 2006. A single-molecule method for the quantitation of microRNA gene expression. *Nat. Methods.* 3:41–46. doi:10.1038/nmeth825

Ohtani, N., D.J. Mann, and E. Hara. 2009. Cellular senescence: its role in tumor suppression and aging. *Cancer Sci.* 100:792–797. doi:10.1111/j.1349-7006.2009.01123.x

Ota, H., E. Tokunaga, K. Chang, M. Hikasa, K. Iijima, M. Eto, K. Kozaki, M. Akishita, Y. Ouchi, and M. Kaneki. 2006. Sirt1 inhibitor, Sirtinol, induces senescence-like growth arrest with attenuated Ras-MAPK signaling in human cancer cells. *Oncogene.* 25:176–185.

Pandey, D.P., and D. Picard. 2009. miR-22 inhibits estrogen signaling by directly targeting the estrogen receptor alpha mRNA. *Mol. Cell. Biol.* 29:3783–3790. doi:10.1128/MCB.01875-08

Poliseno, L., L. Pitto, M. Simili, L. Mariani, L. Riccardi, A. Ciucci, M. Rizzo, M. Evangelista, A. Mercatanti, P.P. Pandolfi, and G. Rainaldi. 2008. The proto-oncogene LRF is under post-transcriptional control of MiR-20a: implications for senescence. *PLoS ONE.* 3:e2542. doi:10.1371/journal.pone.0002542

Ricarte-Filho, J.C., C.S. Fuziwara, A.S. Yamashita, E. Rezende, M.J. da-Silva, and E.T. Kimura. 2009. Effects of let-7 microRNA on cell growth and differentiation of papillary thyroid cancer. *Transl Oncol.* 2:236–241.

Ruas, M., F. Gregory, R. Jones, R. Poolman, M. Starborg, J. Rowe, S. Brookes, and G. Peters. 2007. CDK4 and CDK6 delay senescence by kinase-dependent and p16INK4a-independent mechanisms. *Mol. Cell. Biol.* 27:4273–4282. doi:10.1128/MCB.02286-06

Schmitt, C.A. 2007. Cellular senescence and cancer treatment. *Biochim. Biophys. Acta.* 1775:5–20.

Solomon, J.M., R. Pasupuleti, L. Xu, T. McDonagh, R. Curtis, P.S. DiStefano, and L.J. Huber. 2006. Inhibition of SIRT1 catalytic activity increases p53 acetylation but does not alter cell survival following DNA damage. *Mol. Cell. Biol.* 26:28–38. doi:10.1128/MCB.26.1.28-38.2006

Sun, F., H. Fu, Q. Liu, Y. Tie, J. Zhu, R. Xing, Z. Sun, and X. Zheng. 2008. Downregulation of CCND1 and CDK6 by miR-34a induces cell cycle arrest. *FEBS Lett.* 582:1564–1568. doi:10.1016/j.febslet.2008.03.057

Tahara, H., M. Kusunoki, Y. Yamanaka, S. Matsumura, and T. Ide. 2005. G-tail telomere HPA: simple measurement of human single-stranded telomeric overhangs. *Nat. Methods.* 2:829–831. doi:10.1038/nmeth797

Takakura, S., N. Mitsutake, M. Nakashima, H. Namba, V.A. Saenko, T.I. Rogounovitch, Y. Nakazawa, T. Hayashi, A. Ohtsuru, and S. Yamashita. 2008. Oncogenic role of miR-17-92 cluster in anaplastic thyroid cancer cells. *Cancer Sci.* 99:1147–1154. doi:10.1111/j.1349-7006.2008.00800.x

Takeshita, F., L. Patrawala, M. Osaki, R.U. Takahashi, Y. Yamamoto, N. Kosaka, M. Kawamata, K. Kelnar, A.G. Bader, D. Brown, and T. Ochiya. 2010. Systemic delivery of synthetic microRNA-16 inhibits the growth of metastatic prostate tumors via downregulation of multiple cell-cycle genes. *Mol. Ther.* 18:181–187. doi:10.1038/mt.2009.207

Tapias, A., C.J. Ciudad, I.B. Roninson, and V. Noé. 2008. Regulation of Sp1 by cell cycle related proteins. *Cell Cycle.* 7:2856–2867. doi:10.4161/cc.7.18.6671

Tazawa, H., N. Tsuchiya, M. Izumiya, and H. Nakagama. 2007. Tumor-suppressive miR-34a induces senescence-like growth arrest through modulation of the E2F pathway in human colon cancer cells. *Proc. Natl. Acad. Sci. USA.* 104:15472–15477. doi:10.1073/pnas.0707351104

Ting, Y., D.J. Medina, R.K. Strair, and D.G. Schaar. 2010. Differentiation-associated miR-22 represses Max expression and inhibits cell cycle progression. *Biochem. Biophys. Res. Commun.* 394:606–611. doi:10.1016/j.bbrc.2010.03.030

Tryndyak, V.P., S.A. Ross, F.A. Beland, and I.P. Pogribny. 2009. Down-regulation of the microRNAs miR-34a, miR-127, and miR-200b in rat liver during hepatocarcinogenesis induced by a methyl-deficient diet. *Mol. Carcinog.* 48:479–487. doi:10.1002/mc.20484

Visone, R., P. Pallante, A. Vecchione, R. Cirombella, M. Ferracin, A. Ferraro, S. Volinia, S. Coluzzi, V. Leone, E. Borbone, et al. 2007. Specific microRNAs are downregulated in human thyroid anaplastic carcinomas. *Oncogene.* 26:7590–7595. doi:10.1038/sj.onc.1210564

Wang, G., W. Mao, S. Zheng, and J. Ye. 2009. Epidermal growth factor receptor-regulated miR-125a-5p—a metastatic inhibitor of lung cancer. *FEBS J.* 276:5571–5578. doi:10.1111/j.1742-4658.2009.07238.x

Xiong, J., Q. Du, and Z. Liang. 2010. Tumor-suppressive microRNA-22 inhibits the transcription of E-box-containing c-Myc target genes by silencing c-Myc binding protein. *Oncogene.* 29:4980–4988. doi:10.1038/onc.2010.241

厚生労働科学研究費補助金

肝炎等克服緊急対策研究事業

自然免疫細胞リモデリングによる ウイルス性肝炎の新規治療法の開発

平成22年度～平成24年度　総合研究報告書

（2/2冊）

研究代表者　　大段　秀樹

平成25（2013）年5月

厚生労働科学研究費補助金

肝炎等克服緊急対策研究事業

自然免疫細胞リモデリングによるウイルス性肝炎の新規治療法の開発

平成 22 年度～平成 24 年度　総合研究報告書

（2/2 冊）

研究代表者　　大段　秀樹

平成 25（2013）年 5 月

Journal of Gastroenterology and Hepatology

JGHF

doi:10.1111/jgh.12057

HEPATOLOGY

Characteristics of elderly hepatitis C virus-associated hepatocellular carcinoma patients

Takashi Kumada,* Hidenori Toyoda,* Seiki Kiriyama,* Makoto Tanikawa,* Yasuhiro Hisanaga,* Akira Kanamori,* Toshifumi Tada* and Junko Tanaka†

*Department of Gastroenterology, Ogaki Municipal Hospital, Ogaki, Gifu, and †Department of Epidemiology, Infectious Disease Control and Prevention, Graduate School of Biomedical Sciences, Hiroshima University, Hiroshima, Japan

Key words
alanine aminotransferase (ALT), alpha-fetoprotein (AFP), average integration value of ALT, elderly patient, hepatitis C virus (HCV), hepatocellular carcinoma (HCC), platelet count, propensity score.

Accepted for publication 14 October 2012.

Correspondence
Dr Takashi Kumada, Department of Gastroenterology, Ogaki Municipal Hospital, 4-86, Minaminokawa-cho, Ogaki, Gifu 503-8052, Japan. Email: hosp3@omh.ogaki.gifu.jp

Financial support: This work was supported by Health and Labour Sciences Research Grants (Research on Hepatitis) from the Ministry of Health, Labour and Welfare of Japan.

Declaration of conflict of interest: The authors report no conflicts of interest.

Abstract

Background and Aim: The average age of hepatitis C virus (HCV)-related hepatocellular carcinoma (HCC) patients has been rising in Japan. We evaluate characteristics of HCV-positive patients who develop HCC in older age to determine an optimal surveillance strategy.

Methods: A total of 323 patients with three or more years of follow-up before HCC diagnosis and 323 propensity-matched controls without HCC were studied. HCC patients were classified into four groups according to age at the time of HCC diagnosis: group A (≤ 60 years, $n = 36$), group B (61–70 years, $n = 115$), group C (71–80 years, $n = 143$), and group D (> 80 years, $n = 29$). Clinical and laboratory data were compared.

Results: Platelet counts were significantly higher in the older groups at HCC diagnosis ($P < 0.0001$). The rate of platelet counts decline was lower in older groups ($P = 0.0107$). The average integration value of serum alanine aminotransferase (ALT) in groups A, B, C, and D were 80.9 IU/L, 62.3 IU/L, 59.0 IU/L, and 44.9 IU/L, respectively ($P < 0.0001$). In older patients (≥ 65 years old), cirrhosis and average integration value of ALT were significantly associated with hepatocarcinogenesis, but platelet count was not.

Conclusion: Elderly HCV-positive patients (≥ 65 years old) with low ALT values developed HCC regardless of their platelet counts. These findings should be taken into account when designing the most suitable HCC surveillance protocol for this population.

Introduction

Hepatocellular carcinoma (HCC) is one of the most common malignancies, particularly in southern and eastern Asia. In Japan, HCC is the third leading cause of cancer death in men, behind lung and stomach cancer. In women, HCC is the fifth leading cause of cancer death during the past decade, behind colon, stomach, lung, and breast cancer.[1] Hepatitis C virus (HCV) infection accounts for approximately 75–80% of cases. Each year, HCC develops in 6–8% of patients with HCV-associated cirrhosis.[2]

In Japan, screening the blood supply for HCV, which commenced in November 1989 and began using second-generation enzyme immunoassays in February 1992, decreased the risk of post-transfusion hepatitis from more than 50% in the 1960s to virtually zero presently.[3] The age of Japanese patients diagnosed with HCC has been steadily increasing. Up to 1999, the majority of HCC mortalities occurred in patients under 69 years of age, but in 2000 more than half of HCC patients were over the age of 70.[1] This aging trend is also observed in HCV patients undergoing interferon-based therapy in Japan.[4] In contrast, HCV infection in the United States and other western countries is most prevalent among persons 30 to 50 years of age,[5] and the incidence of HCV-associated HCC is expected to rise. As a country with more experience with HCV-associated HCC, Japan's long-term experience can be helpful in planning strategies to contain HCV infection and to cope with its long-term sequelae worldwide.

The aim of this study is to evaluate characteristics of HCV-positive patients who develop HCC in older age and to determine an optimal surveillance strategy for these patients.

Materials and methods

Study population. This study cohort was comprised of 6740 consecutive HCV-positive patients (1019 patients with HCC and 5721 patients without HCC) referred to the Department of Gastroenterology at Ogaki Municipal Hospital from January 1990 to December 2006.

There were 323 patients who fulfilled the following inclusion criteria out of 1019 HCC patients: (i) detectable HCV-RNA for at least six months, (ii) no evidence of hepatitis B virus infection; (iii) other possible causes of chronic liver disease were ruled out

(no history of hepatotoxic drug use, and negative tests for autoimmune hepatitis, primary biliary cirrhosis, hemochromatosis, and Wilson's disease); (iv) a follow-up period of greater than three years before HCC diagnosis; (v) no interferon therapy within the last 12 months; and (vi) serum alanine aminotransferase (ALT) measurements taken more than twice yearly. The patients were classified into four groups according to age at the time of HCC diagnosis: group A (≤ 60 years, $n = 36$), group B (61–70 years, $n = 115$), group C (71–80 years, $n = 143$), and group D (> 80 years, $n = 29$).

Of the 5721 patients who have not developed HCC, 3275 patients fulfilled the same inclusion criteria. To reduce the confounding effects of covariates, we used propensity scores to match HCC patients with unique control patients based on age, sex, Child-Pugh classification at the start of follow-up, and follow-up duration. We were able to match 323 patients with HCC to 323 patients without HCC. The patients were classified into four groups according to age at the end of follow-up: group A' (≤ 60 years, $n = 30$), group B' (61–70 years, n = 114), group C' (71–80 years, $n = 136$), and group D' (> 80 years, $n = 43$).

The start of follow-up was defined as the date a patient first visited our hospital and ended on the date of HCC diagnosis for the HCC patients, or the date of the last visit at our hospital or December 31, 2010, whichever occurred earlier, in control patients.

Histological examinations were performed in 234 out of 646 patients. Cirrhosis was diagnosed pathologically in 120 patients. The remaining 412 patients were evaluated with ultrasonography (US) and biochemical tests.[6–8] Patients who did not satisfy the criteria for cirrhosis were classified as having chronic hepatitis for the purposes of this study. All together, 288 out of 646 patients were diagnosed with chronic hepatitis, and 358 were diagnosed with cirrhosis.

The study protocol was approved by the Ethics Committee at Ogaki Municipal Hospital in January 22, 2009 and complied with the Helsinki Declaration. Each patient provided written informed consent.

Laboratory test for liver disease and virologic markers. Platelet counts, prothrombin time, and serum levels of ALT, albumin, total bilirubin, alpha-fetoprotein (AFP), *lens culinaris* agglutinin–reactive fraction of AFP (AFP-L3%), and des-γ-carboxy prothrombin (DCP) were determined at the start of follow-up. ALT is expressed as an average integration value.[6] Serum AFP concentration was determined with a commercially available kit. AFP-L3 was measured by lectin-affinity electrophoresis and antibody-affinity blotting with the AFP Differentiation Kit L (Wako Pure Chemical Industries, Ltd, Osaka, Japan).[9] DCP was quantified with the Picolumi PIVKA-II kit (Eisai Co., Ltd, Tokyo, Japan).[10] HCV genotype was determined by PCR using genotype-specific primers, and HCV-RNA was quantified (before November 2007; COBAS Amplicor HCV monitor test and after December 2007; COBAS AmpliPrep/COBAS TaqMan HCV test, Roche Diagnostics K.K., Tokyo, Japan).

Alcohol exposure. Past alcohol exposure was estimated based on chart review of drinking patterns over five years. Patients were categorized as either "excessive" or "moderate" alcohol consumers. Excessive alcohol consumers drank over 50 g daily for five years.

Methods of follow-up. All patients received medical examinations at least every six months at our institution. Imaging studies, either US, computed tomography (CT), or magnetic resonance imaging (MRI), were performed at least every six months. When patients were considered to have developed cirrhosis by laboratory data or imaging findings, imaging was performed at three-month intervals.[11]

Diagnosis and treatment of HCC. The diagnosis of HCC was made based on either pathological or clinical and radiological criteria. Histological examination of resected hepatic tumors or US-guided needle biopsy specimens confirmed HCC in 165 patients (resected specimens: 111 patients; biopsy specimens: 54 patients). In the remaining 158 patients, the diagnosis of HCC was made using clinical criteria and imaging findings obtained from B-mode US, CT, MRI, and CT angiography.[12,13]

Tumor staging was performed according to the American Joint Committee on Cancer (AJCC) classification system.[14] In cases where pathologic evaluation was not available, vascular invasion was assessed by dynamic CT and angiography.

Treatment for each patient was individualized according to evidence-based clinical practice guidelines for HCC in Japan.[14] Hepatic resection was performed on 111 patients. Percutaneous ethanol injection therapy was performed in 16 patients. Radiofrequency ablation therapy was performed in 104 patients. Transcatheter arterial chemoembolization was performed in 62 patients. Thirty patients did not undergo treatment because of the patient's wishes or impaired liver function.

Statistical analyses. Statistical analysis was performed with the Statistical Program for Social Science (SPSS ver.18.0 for Windows; SPSS Japan Inc., Tokyo, Japan). Continuous variables are represented as medians (range). The non-parametric Jonckheere–Terpstra test was used to assess continuous variables. The Steel–Dwass or Shirley–Williams multiple comparisons method was applied if the Jonckheere–Terpstra test yielded significant results. The Cochran–Armitage test or the chi-square test was used to assess categorical variables. Actual survival was estimated using the Kaplan–Meier method,[15] and differences were tested with the log-rank test.[16] The Cox proportional hazards model and forward selection method were used to estimate the relative risk of HCC development associated with age, sex, cirrhosis, alcohol consumption, diabetes mellitus, effect of prior interferon therapy, platelet count, AFP at the start of follow-up, and average integration value of ALT, and the annual rate of platelet count decline. Statistical significance was set at $P < 0.05$.

Results

Clinical features at baseline. The clinical profiles of the HCC patients at the start of follow-up are shown in Table 1. There was a higher proportion of women diagnosed with HCC at a later age ($P = 0.0016$); the percentage of women in groups A, B, C, and

Table 1 Profile of HCV-infected HCC patients at the start of follow-up

	Group A ($n = 36$)	Group B ($n = 115$)	Group C ($n = 143$)	Group D ($n = 29$)	P
Sex (female/male)	5/31	43/72	63/80	15/14	0.0016
Age at the start of follow-up† (years)	49 (36–57)	59 (47–66)	66 (52–75)	74 (64–80)	< 0.0001
Duration of observation period until HCC diagnosis† (years)	6.4 (3.1–16.7)	6.9 (3.0–15.8)	8.0 (3.0–17.7)	9.3 (3.0–15.7)	0.0003
Alcohol consumption (≥ 50 g per day/< 50 g per day)	9/27	24/91	26/117	2/27	0.0873
History of blood transfusion (present/absent)	6/30	26/89	35/108	2/27	0.8247
Diabetes mellitus (present/absent)	24/12	40/75	51/92	5/24	0.0008
Prior interferon therapy (SVR/non-SVR/absent)	3/17/16	12/32/71	0/15/128	0/1/28	< 0.0001

†Expressed as median (range).
Group A, diagnosis of HCC at age ≤ 60 years; Group B, 61–70 years; Group C, 71–80 years; Group D, > 80 years.
HCC, hepatocellular carcinoma; HCV, hepatitis C virus; SVR, sustained virologic response.

Table 2 Profile of control patients with HCV infection at the start of follow-up

	Group A' ($n = 30$)	Group B' ($n = 114$)	Group C' ($n = 136$)	Group D' ($n = 43$)	P
Sex (female/male)	7/23	48/66	56/80	20/23	0.1175
Age at the start of follow-up† (years)	48 (40–56)	58 (48–67)	66 (54–75)	74 (65–82)	< 0.0001
Duration of observation period until the end of follow-up† (years)	7.0 (3.0–15.5)	7.8 (3.0–18.7)	8.5 (3.0–17.7)	8.5 (3.6–19.1)	0.0064
Alcohol consumption (≥ 50 g per day / < 50 g per day)	8/22	27/87	20/116	3/40	0.0630
History of blood transfusion (present/absent)	5/25	29/85	40/96	2/41	0.1939
Diabetes mellitus (present/absent)	7/23	38/76	47/89	12/31	0.0758
Prior interferon therapy (SVR/non-SVR/absent)	4/15/11	8/34/72	3/20/113	0/1/42	< 0.0001

†Expressed as median (range).
Group A', age ≤ 60 years at the end of follow-up; Group B', 61–70 years; Group C', 71–80 years; Group D', > 80 years.
HCV, hepatitis C virus; SVR, sustained virologic response.

D was 13.9, 37.4, 44.1, and 51.7, respectively. As the patient's age at HCC diagnosis increased, the patient's age at the start of follow-up and the duration of the observation period until HCC diagnosis increased ($P < 0.0001$ and $P = 0.0003$, respectively). Patients who received a diagnosis of HCC at a more advanced age have a significantly decreased incidence of diabetes mellitus and prior interferon therapy ($P = 0.0008$ and $P < 0.0001$, respectively). The clinical profiles of the control patients at the start of follow-up are shown in Table 2. The same tendency between HCC patients and control patients was observed.

Laboratory data of the HCC patients at the start of follow-up are shown in Table 3. Patients diagnosed with HCC at a more advanced age had lower baseline serum ALT and AFP levels ($P < 0.0001$ and $P = 0.0043$, respectively) and higher baseline platelet counts ($P = 0.0032$). In Table 4, the oldest group of control patients had lower baseline serum ALT and AFP levels ($P < 0.0001$ and $P = 0.0261$, respectively); however, no significant differences in baseline platelet count were observed.

The results of the Cox proportional hazards model and forward selection method to test factors associated with the age-related development of HCC to patient age at the start of follow-up are shown in Table 5. Ten covariates including age, sex, cirrhosis, alcohol consumption, diabetes mellitus, effect of prior interferon therapy, platelet count, baseline AFP, average integration value of ALT, and the annual rate of platelet count decline were studied. Age, cirrhosis, average integration value of ALT, platelet count, and AFP were significantly associated with hepatocarcinogenesis. However, only cirrhosis and average integration value of ALT were selected as factors significantly associated with hepatocarcinogenesis in patients ≥ 65 or 70 years old. Platelet count was not a significant factor.

Clinical features at the time of HCC diagnosis. Platelet counts at the time of HCC diagnosis in groups A, B, C, and group D were $72 \times 10^3/mm^3$ (40–192), $84 \times 10^3/mm^3$ (28–256), $99 \times 10^3/mm^3$ (31–355), and $119 \times 10^3/mm^3$ (58–232), respectively. There is a statistically significant trend toward higher platelet counts as the age at HCC diagnosis increases ($P < 0.0001$). In contrast, platelet counts at the end of follow-up in groups A', B', C', and D' were $194 \times 10^3/mm^3$ (44–543), $172 \times 10^3/mm^3$ (40–484), $177 \times 10^3/mm^3$ (21–415), and $193 \times 10^3/mm^3$ (52–429), respectively. There is no significant difference between the four groups of control patients ($P = 0.4772$). The annual rate of decline in platelet count, calculated as [platelet count at the start of the study period—platelet count at the time of HCC diagnosis]/duration of the observation period until the diagnosis of HCC, decreased significantly as the age at HCC diagnosis increased, and the annual rate of decline in platelet count, calculated as [platelet count at the start of study period—platelet count at the end of follow-up]/duration of observation period until the end of follow-up in control patients, did not increase significantly as the age at the end of follow-up increased (Fig. 1, $P = 0.0247$ and 0.1571, respectively). The annual rate of platelet count decline was

Table 3 Baseline laboratory data of HCV-infected HCC patients

	Group A ($n = 36$)	Group B ($n = 115$)	Group C ($n = 143$)	Group D ($n = 29$)	*P*
Platelet count† ($\times 10^3/mm^3$)	104 (34–249)	114 (29–253)	125 (44–307)	124 (70–201)	0.0032
Prothrombin time† (%)	87 (52–129)	88 (24–119)	85 (22–128)	86 (45–129)	0.6062
Total bilirubin† (mg/dL)	0.8 (0.3–1.8)	0.7 (0.2–4.7)	0.7 (0.3–6.7)	0.6 (0.2–1.3)	0.4583
ALT† (IU/L)	125 (24–361)	76 (18–387)	64 (8–154)	44 (17–221)	< 0.0001
Child-Pugh classification[17] (A or B/C)	33/3	103/12	130/13	24/5	0.5512
HCV genotype‡ (1/2)	26/6	66/24	75/29	15/6	0.4083
HCV viral concentration† (log copies/mL)	5.7 (2.7–8.0)	5.0 (2.0–8.0)	5.4 (2.0–6.9)	5.5 (3.0–7.0)	0.4952
AFP† (ng/mL)	13.5 (1.8–163.4)	8.4 (1.9–583.4)	7.2 (1.0–372.3)	4.8 (1.2–141.5)	0.0043
AFP-L3† (%)	0 (0–56.3)	0 (0–43.6)	0 (0–15.2)	0 (0–7.0)	1.0000
DCP† (mAU/mL)	19 (10–154)	19 (10–367)	17 (10–745)	15 (10–182)	0.0958
Cirrhosis (present/absent)	31/5	95/20	112/31	21/8	0.0903

†Expressed as median (range).
‡Data were unavailable for 76 patients.
AFP, alpha-fetoprotein; AFP-L3, *lens culinaris* agglutinin–reactive fraction of AFP; ALT, alanine aminotransferase; DCP, des-γ-carboxy prothrombin; Group A, diagnosis of HCC at age ≤ 60 years; Group B, 61–70 years; Group C, 71–80 years; Group D, > 80 years; HCC, hepatocellular carcinoma; HCV, hepatitis C virus.

Table 4 Baseline laboratory data of control patients with HCV infection

	Group A′ ($n = 30$)	Group B′ ($n = 114$)	Group C′ ($n = 136$)	Group D′ ($n = 43$)	*P*
Platelet count† ($\times 10^3/mm^3$)	204 (58–375)	180 (40–540)	187 (51–484)	196 (52–418)	0.4301
Prothrombin time† (%)	100 (52–138)	96 (38–153)	96 (48–144)	95 (47–145)	0.3435
Total bilirubin† (mg/dL)	0.5 (0.2–1.2)	0.4 (0.2–5.3)	0.4 (0.2–5.3)	0.3 (0.2–1.5)	0.6298
ALT† (IU/L)	53 (12–131)	46 (5–490)	35 (8–484)	22 (2–199)	< 0.0001
Child-Pugh classification[17] (A or B/C)	30/0	103/11	128/8	40/3	0.1088
HCV genotype‡ (1/2)	15/10	60/23	66/25	12/5	0.0869
HCV viral concentration† (log copies/mL)	5.9 (2.7–6.6)	5.7 (2.7–7.3)	5.8 (2.0–7.0)	5.1 (3.0–6.6)	0.1130
AFP† (ng/mL)	4.3 (0.8–156.3)	3.1 (0.8–170.3)	3.1 (0.8–219.2)	2.0 (0.8–29.2)	0.0261
AFP-L3† (%)	0 (0–26.9)	0 (0–34.2)	0 (0–41.4)	0 (0–5.2)	1.0000
DCP† (mAU/mL)	22 (10–122)	19 (10–487)	19 (10–503)	16 (10–30)	0.2549
Cirrhosis (present/absent)	5/25	35/79	48/88	11/32	0.1201

†expressed as median (range).
‡Data were unavailable for 107 patients.
AFP, alpha-fetoprotein; AFP-L3, *lens culinaris* agglutinin–reactive fraction of AFP; ALT, alanine aminotransferase; DCP, des-γ-carboxy prothrombin; Group A′, age ≤ 60 years at the end of follow-up; Group B′, 61–70 years; Group C′, 71–80 years; Group D′, > 80 years; HCV, hepatitis C virus.

Table 5 Factors associated with the development of HCC according to the age at start of follow-up in multivariate analysis

		All patients ($n = 646$) *hazard ratio (95% CI)*	≥ 60 years ($n = 428$) *hazard ratio (95% CI)*	≥ 65 years ($n = 255$) *hazard ratio (95% CI)*	≥ 70 years ($n = 92$) *hazard ratio (95% CI)*
Age (years)	≤ 60	1			
	> 60, ≤ 70	1.600 (1.240–2.064)			
	> 70	2.738 (1.858–4.036)			
Cirrhosis	Absent	1	1	1	1
	Present	2.165 (1.575–2.978)	2.269 (1.554–3.311)	2.734 (1.724–4.336)	2.962 (1.200–7.310)
Average integration value of ALT (IU/L)	≤ 20	1	1	1	1
	> 20, ≤ 40	4.239 (1.336–13.800)	4.885 (1.179–20.249)	5.243 (1.253–22.020)	12.162 (1.549–95.496)
	> 40, ≤ 60	5.518 (1.725–17.648)	6.661 (1.619–23.397)	6.739 (1.610–28.250)	6.797 (0.854–54.080)
	> 60, ≤ 80	7.182 (2.230–23.130)	9.362 (2.268–38.641)	12.265 (2.867–56.471)	11.183 (1.400–89.317)
	> 80	10.211 (3.175–33.031)	12.249 (2.494–50.884)	13.087 (2.962–57.815)	11.052 (0.964–126.671)
Platelet count ($\times 10^3/mm^3$)	≥ 150	1	1		
	< 150	1.644 (1.237–2.186)	1.728 (1.240–2.408)		
AFP* (ng/mL)	≤ 10	1			
	> 10, ≤ 20	1.406 (1.002–1.971)			
	> 20	1.609 (1.214–2.132)			

AFP, alpha-fetoprotein; ALT, alanine aminotransferase; CI, confidence interval; HCC, hepatocellular carcinoma.

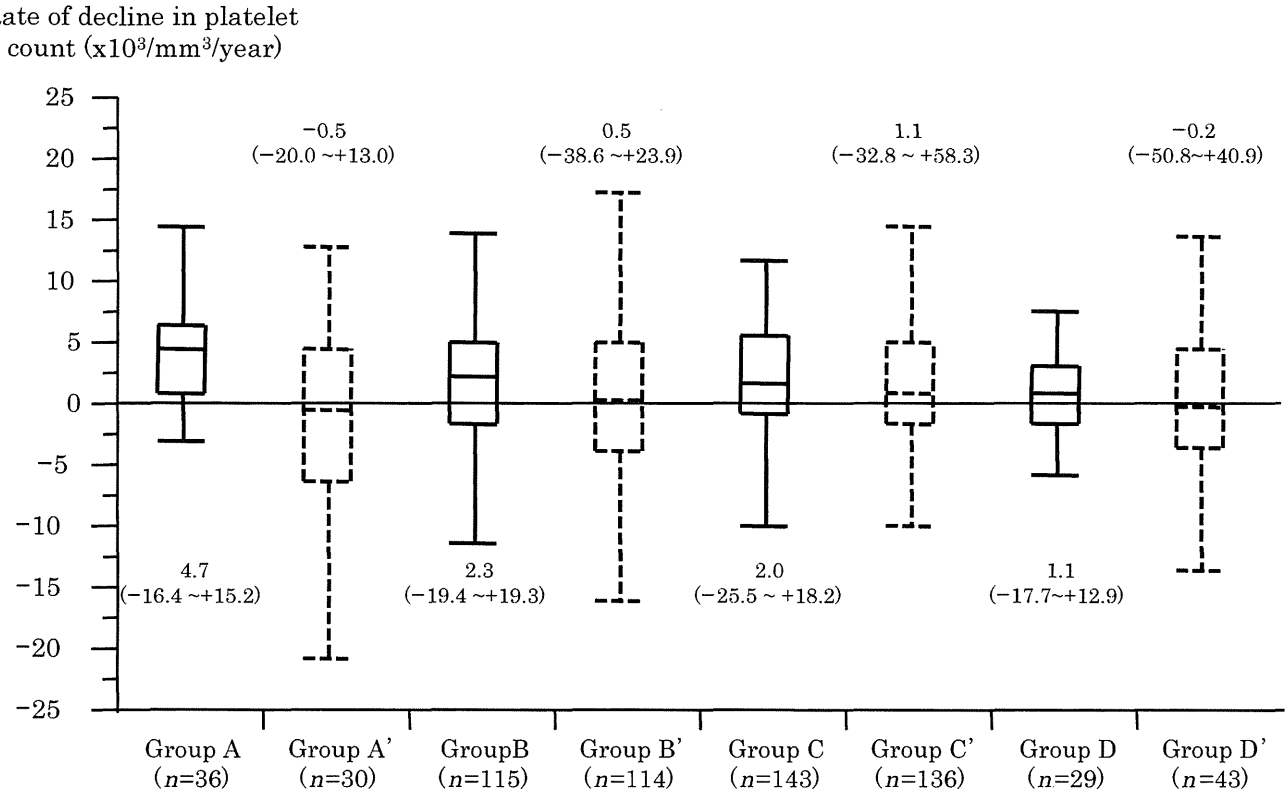

Figure 1 Rate of decline in platelet count prior to hepatocellular carcinoma (HCC) diagnosis in HCC patients and prior to the end of follow-up in control patients. The annual rate of platelet count decline in the period prior to HCC diagnosis was lower in the groups that were older at the time of HCC diagnosis. In control patients, there was no trend toward higher annual rates of platelet count decline in the period prior to the end of follow-up when the patients were classified by age ($P = 0.0247$ and 0.1571, respectively, Jonckheere-Terpstra Test). Group A, HCC diagnosed at age ≤ 60 years; group B, 61–70 years; group C, 71–80 years; group D, > 80 years. group A', control patients ≤ 60 years old at the end of follow-up; group B', 61–70 years; group C', 71–80 years; group D', > 80 years. The annual rate of platelet count decline was significantly lower in group A' than in group A ($P = 0.0039$); however, there were no significant differences when HCC patients in other age groups were compared to their respective matched controls.

lower in group A' than in group A ($P = 0.0039$), and there were no significant differences between group B and group B', group C and group C', and group D and group D'.

The average integration value of ALT in groups A, B, C, and D was 80.9 IU/L (25.3–179.3), 62.3 IU/L (14.5–167.9), 59.0 IU/L (9.9–134.1), and 44.9 IU/L (22.7–91.9), respectively. The average integration value of ALT was significantly lower in patients diagnosed with HCC at an older age (Fig. 2, $P < 0.0001$). There was a similar trend among control patients (Fig. 2, $P < 0.0001$). The average integration values of ALT in groups A', B', C', and D' were significantly lower than in groups A, B, C, and D, respectively ($P < 0.0001$).

Patient profiles at the time of HCC diagnosis are shown in Table 6. There were no significant differences in tumor characteristics and levels of tumor markers among the age groups. Fewer patients in Group D underwent hepatic resection ($P = 0.0293$).

Survival rates according to age at HCC diagnosis. Five and 10-year cumulative survival rates of groups A, B, C, and D were 44.2%, 58.2%, 44.3%, and 33.3% and 22.7%, 31.2%, 26.6%, and not available, respectively (Fig. 3). There were no significant differences in the cumulative survival rate among the four groups.

Discussion

In Japan, the average age of patients with chronic hepatitis, cirrhosis, or HCV-associated HCC is increasing. The number of deaths due to these diseases is also increasing. The age-specific prevalence of HCV seropositivity in the USA is about 30 years below that in Japan; thus, a majority of patients in the USA with chronic HCV infection will reach an advanced age in the near future.[3]

In our study, elderly HCC patients have high platelet counts and low ALT values. In addition, multivariate analysis using propensity-matched control patients revealed that the presence of cirrhosis and high ALT levels (> 20 IU/L) are significantly associated with the development of HCC. However, platelet count is not significantly associated with hepatocarcinogenesis in elderly HCV carriers (≥ 65 years). Physicians should be aware that patients aged 65 years or older could develop HCC regardless of their platelet count.

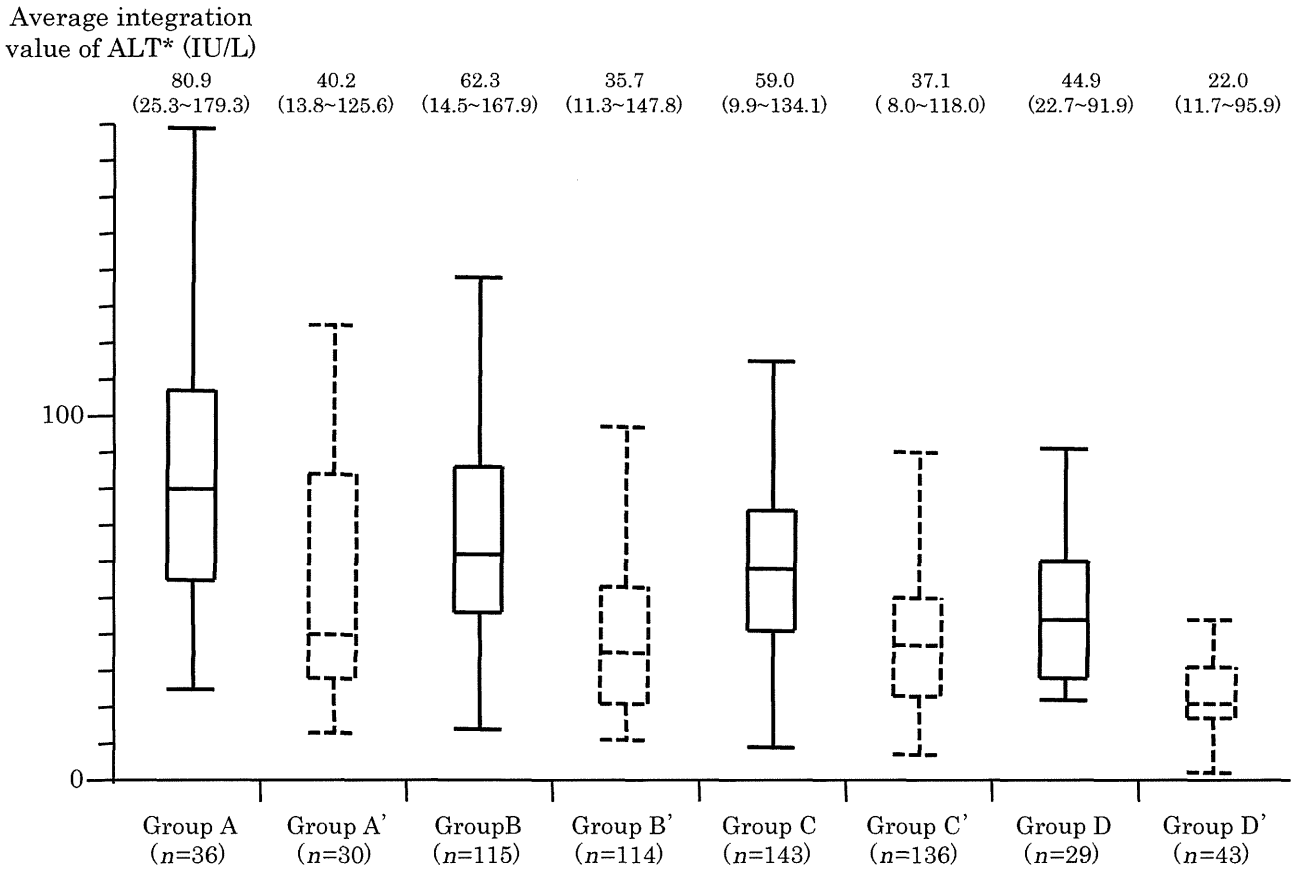

Figure 2 Average integration values of alanine aminotransferase (ALT) prior to HCC diagnosis in HCC patients and prior to the end of follow-up in control patients. Patients who were older at the time of HCC diagnosis had lower average integration values of ALT in the period prior to HCC diagnosis. In control patients, the average integration values of ALT in the period prior to the end of follow-up were lower in the groups that were older at the end of follow-up ($P < 0.0001$ and < 0.0001, respectively, Jonckheere-Terpstra Test). Average integration values of ALT in groups A', B', C', and D' were significantly lower than in groups A, B, C, and D, respectively ($P < 0.0001$).

Table 6 Profile of HCV-infected HCC patients at the time of HCC diagnosis

	Group A ($n = 36$)	Group B ($n = 115$)	Group C ($n = 143$)	Group D ($n = 29$)	P
AFP† (ng/mL)	23.9 (0.8–500)	19.8 (0.6–10500)	12.8 (0.8–12680)	17.8 (0.8–99720)	0.2347
AFP-L3† (%)	0 (0–89)	0 (0–87.2)	0 (0–81.0)	0 (0–40.7)	1.0000
DCP† (mAU/mL)	36 (10–36164)	35 (10–5941)	32 (10–50904)	24 (10–6229)	0.5650
Tumor size† (cm)	2.0 (0.8–10.0)	2.0 (0.3–8.8)	2.0 (0.6–11.4)	2.3 (1.0–9.0)	0.3754
Number of tumors†	1 (1–6)	1 (1–8)	1 (1–10)	1 (1–4)	1.0000
Portal thrombus (present/absent)	2/34	3/112	6/137	0/29	0.3293
Stage (1/2/3/4)	14/15/5/2	41/53/21/0	50/61/29/3	10/12/7/0	0.4957
Initial treatment (HR/PT/TACE/none)	9/18/4/5	47/44/16/8	51/47/33/12	4/11/9/5	0.0293

†Expressed as median (range).

AFP, α-fetoprotein; AFP-L3, *lens culinaris* agglutinin–reactive fraction of AFP; DCP, des-γ-carboxy prothrombin; Group A, diagnosis of HCC at age ≤ 60 years; Group B, 61–70 years; Group C, 71–80 years; Group D, > 80 years; HCC, hepatocellular carcinoma; HCV, hepatitis C virus; HR, hepatic resection; PT; percutaneous treatment including ethanol injection therapy, microwave coagulation therapy, and radiofrequency ablation therapy; TACE, transcatheter arterial chemoembolization.

The male-to-female ratio of HCC patients in Japan has decreased from 4.5 in 1984–1985 to 2.5 in 2002–2003.[1] It is well known that the mean age of female HCC patients with HCV infection is higher than that of males.[18,19] The increased proportion of female patients is considered a result of more older patients with HCV-related HCC. In our study, the proportion of female patients was the highest in group D. Further investigation of the role of sex in hepatocarcinogenesis is needed.